

Development of Robust Iris Localization and Impairment Pruning Schemes

Sambit Bakshi



**Department of Computer Science and Engineering
National Institute of Technology Rourkela
Rourkela-769 008, Odisha, India**

Development of Robust Iris Localization and Impairment Pruning Schemes

Thesis submitted in

May 2011

to the department of

Computer Science and Engineering

of

National Institute of Technology Rourkela

in partial fulfillment of the requirements

for the degree of

Master of Technology

in

Computer Science and Engineering

by

Sambit Bakshi

[Roll No. 209CS2082]

under the guidance of

Prof. Banshidhar Majhi



**Department of Computer Science and Engineering
National Institute of Technology Rourkela
Rourkela-769 008, Odisha, India**



Department of Computer Science & Engineering
National Institute of Technology Rourkela

Rourkela-769 008, Odisha, India.

www.nitrkl.ac.in

Dr. Banshidhar Majhi

Professor

May 20, 2011

Certificate

This is to certify that the work in the thesis entitled *Development of Robust Iris Localization and Impairment Pruning Schemes* by *Sambit Bakshi*, bearing Roll No. 209CS2082, is a record of an original research work carried out by him under my supervision and guidance in partial fulfilment of the requirements for the award of the degree of *Master of Technology in Computer Science and Engineering*. Neither this thesis nor any part of it has been submitted for any degree or academic award elsewhere.

Banshidhar Majhi

ROURKELA

Acknowledgment

O Lord, who lends me life, lend me a heart replete with thankfulness.

- William Shakespeare

I would like to express my earnest gratitude to my thesis guide, Prof. Banshidhar Majhi for believing in my ability to work on the challenging domain of biometric security. His profound insights has enriched my research work. The flexibility of work he has offered me has deeply encouraged me producing the research. I am also grateful to Dr. Pankaj Kumar Sa for being a source of support and motivation for carrying out quality work.

My hearty thanks goes to Ms. Hunny Mehrotra for consistently showing me innovative research directions for the entire period of carrying out the research and helping me in shaping up the thesis. I am indebted to all the professors, co-researchers, batch mates and friends at National Institute of Technology Rourkela for their active or hidden cooperation. Their contributions have always been unfeigned. I cannot resist myself quoting my thanks to the developers of L^AT_EX compiler for making the thesis writing an experience indeed.

I would conclude with my deepest gratitude to my parents and all my loved ones. My full dedication to the work would have not been possible without their blessings and moral support. This thesis is a dedication to them who did not forget to keep me in their hearts when I could not be beside them.

ROURKELA

Sambit Bakshi

Please do not print this thesis or any part of it unless you really need to.

Save paper, save green, save life.

Abstract

Iris is the sphincter having flowery pattern around pupil in the eye region. The high randomness of the pattern makes iris unique for each individual and iris is identified by the scientists to be a candidate for automated machine recognition of identity of an individual. The morphogenesis of iris is completed while baby is in mother's womb; hence the iris pattern does not change throughout the span of life of a person. It makes iris one of the most reliable biometric traits.

Localization of iris is the first step in iris biometric recognition system. The performance of matching is dependent on the accuracy of localization, because mislocalization would lead the next phases of biometric system to malfunction. The first part of the thesis investigates choke points of the existing localization approaches and proposes a method of devising an adaptive threshold of binarization for pupil detection. The thesis also contributes in modifying conventional integrodifferential operator based iris detection and proposes a modified version of it that uses canny detected edge map for iris detection.

The other part of the thesis looks into pros and cons of the conventional global and local feature matching techniques for iris. The review of related research works on matching techniques leads to the observation that local features like Scale Invariant Feature Transform (SIFT) gives satisfactory recognition accuracy for good quality images. But the performance degrades when the images are occluded or taken non-cooperatively. As SIFT matches keypoints on the basis of 128-D local descriptors, hence it sometimes falsely pairs two keypoints which are from different portions of two iris images. Subsequently the need for filtering or pruning of faulty SIFT pairs is felt. The thesis proposes two methods of filtering impairments (faulty pairs) based on the knowledge of spatial information of the keypoints. The two proposed pruning algorithms (Angular Filtering and Scale Filtering) are applied separately and applied in union to have a complete comparative analysis of the result of matching.

Keywords: Iris recognition, localization, SIFT, matching, filtering, pruning of SIFT pairs.

Contents

Certificate	ii
Acknowledgement	iii
Abstract	iv
List of Algorithms	vii
List of Figures	viii
List of Tables	x
List of Acronyms	xi
1 Introduction	1
1.1 About Iris Biometrics	2
1.2 Motivation	3
1.3 Problem Definition	4
1.4 Performance Measures Used	9
1.5 Iris Databases	12
1.6 Experimental Setup	13
1.7 Thesis Organization	13
2 Iris localization Using Adaptive Thresholding	14
2.1 Literature Survey	15
2.2 Proposed Adaptive Thresholding	17

2.3	Pupil Detection	19
2.4	Iris Detection	22
2.4.1	Proposed Iris Detection	24
2.5	Experimental Results	26
2.6	Summary	28
3	Postmatch Pruning of SIFT Impairments	30
3.1	Related Works	31
3.2	Iris Feature Extraction using SIFT	33
3.2.1	Scale Space Extrema Detection	33
3.2.2	Keypoint Localization	34
3.2.3	Orientation Assignment	35
3.2.4	Keypoint Descriptor Computation	36
3.3	Proposed Postmatching Pruning Approach	36
3.3.1	Nearest Neighbor SIFT Keypoint Pairing	36
3.3.2	Proposed Filtering of Keypoints	37
3.4	Experimental Results	43
3.4.1	Experiment I: Applying conventional SIFT	44
3.4.2	Experiment II: Applying Angular filtering	44
3.4.3	Experiment III: Applying Scale filtering	45
3.4.4	Experiment IV: Applying combined Angular and Scale filtering	45
3.5	Summary	46
4	Conclusions and Future Work	51
	Bibliography	53
	Dissemination	57

List of Algorithms

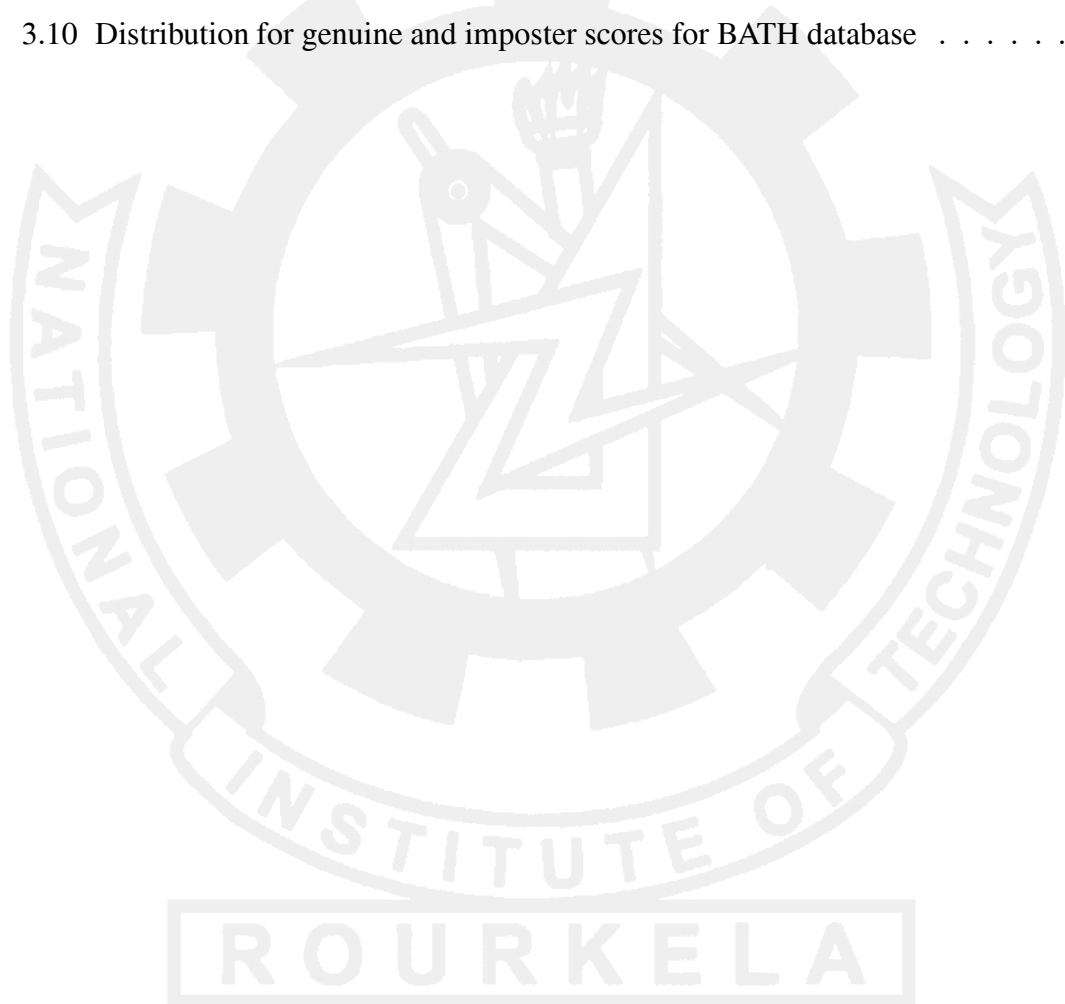
2.1	Proposed adaptive thresholding	20
2.2	Pupil detection	22
2.3	Conventional intensity image based circular summation iris detection	23
2.4	Proposed canny detected image based circular summation iris detection . . .	25
3.1	Nearest neighbour SIFT keypoint pairing	38
3.2	Proposed filtering of SIFT pairs based on angular information	41
3.3	To find gradient of a keypoint	41
3.4	Proposed filtering of SIFT pairs based on scaling information	43
3.5	To find Euclidean distance of a keypoint from the centre of iris	43



List of Figures

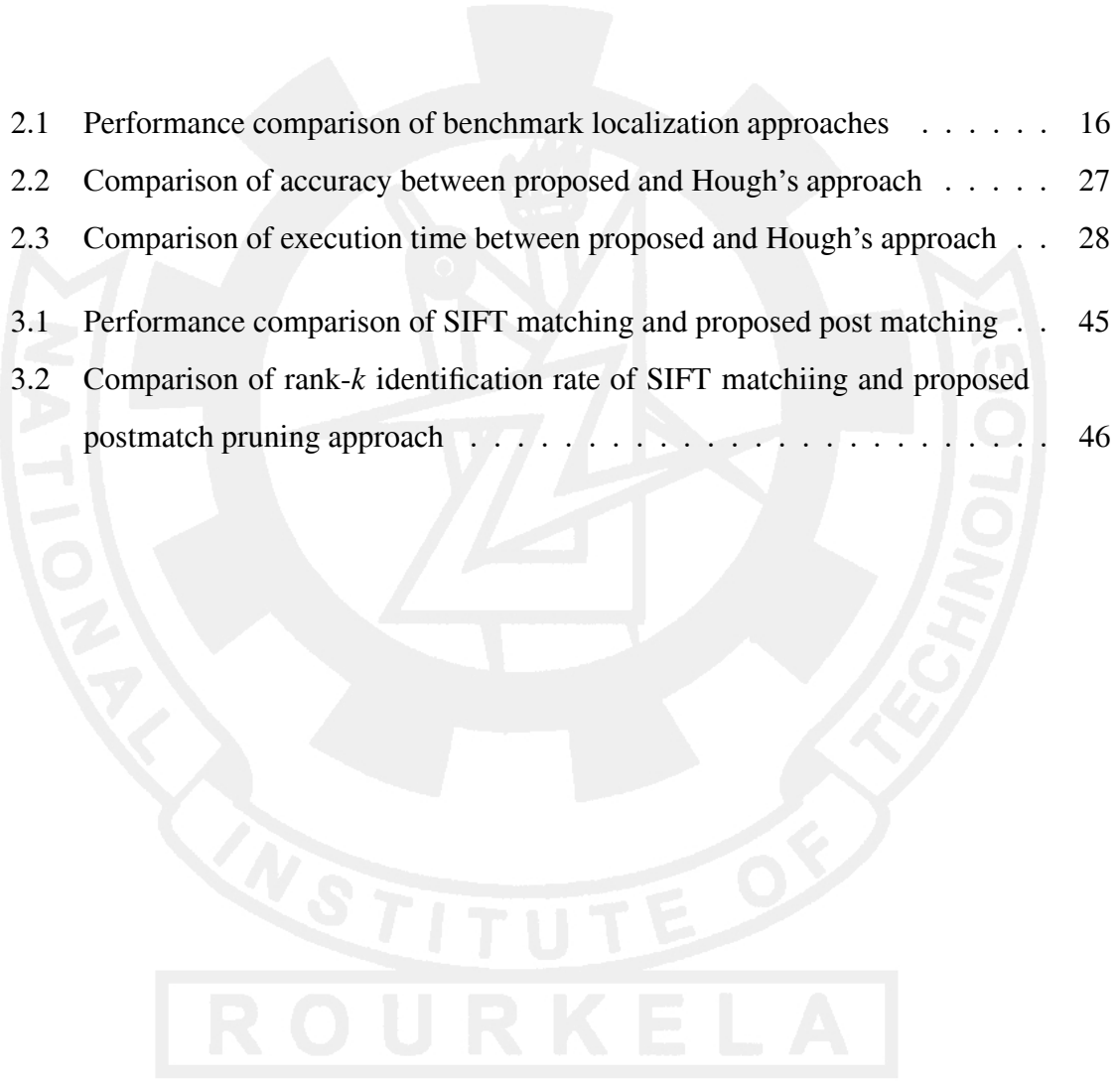
1.1	Eye anatomy	3
1.2	Block diagram of generic biometric system	5
1.3	Domain of proposed Work I in localization	6
1.4	Block diagram of local feature extraction based biometric system	7
1.5	Domain of proposed Work II in post matching	8
1.6	Genuine and imposter matching score distribution of biometric database showing various performance measures	10
2.1	Grid based adaptive thresholding	17
2.2	Change in number of connected components in binarized image with change of threshold	18
2.3	Different binary images obtained with the change in threshold	21
2.4	Steps involved in pupil detection	21
2.5	Steps involved in conventional iris detection	23
2.6	Failure of conventional iris detection algorithm	24
2.7	Steps involved in proposed iris detection	25
2.8	Performance of proposed approach in some non-cooperative scenarios	26
2.9	Illumination invariant localization by the proposed approach	27
2.10	Instances where proposed approach performs better than Hough transform	28
3.1	To find Difference of Gaussian in different octaves of annular iris image	34
3.2	SIFT detected keypoints and oriented descriptor windows around some sample keypoints	35
3.3	Sample impairments generated by SIFT matching	37

3.4	Gradient and Scaling factor computation	39
3.5	Gradient histogram of matched keypoints between two instances of the same subject	39
3.6	Filtered matches obtained by proposed pruning schemes	42
3.7	Accuracy curve, ROC curve, CMC curve for CASIAV3 database	47
3.8	Accuracy curve, ROC curve, CMC curve for BATH database	48
3.9	Distribution for genuine and imposter scores for CASIAV3 database	49
3.10	Distribution for genuine and imposter scores for BATH database	50



List of Tables

2.1	Performance comparison of benchmark localization approaches	16
2.2	Comparison of accuracy between proposed and Hough's approach	27
2.3	Comparison of execution time between proposed and Hough's approach	28
3.1	Performance comparison of SIFT matching and proposed post matching	45
3.2	Comparison of rank- k identification rate of SIFT matching and proposed postmatch pruning approach	46



List of Acronyms

CHT Circular Hough Transform

CMC Cumulative Match Characteristic

DOG Difference of Gaussian

EER Equal Error Rate

FAR False Acceptance Rate

FRR False Rejection Rate

GAR Genuine Acceptance Rate

ROC Receiver Operating Characteristic

SIFT Scale Invariant Feature Transform

SURF Speeded Up Robust Features

ROURKELA

Chapter 1

Introduction

Biometrics is the science of recognizing the identity of an individual based on physiological and behavioural characteristics of the subject. Biometric authentication has evolved from the disadvantages of traditional means of authentication. The problem with token based systems is that the possession could be lost, stolen, forgotten or misplaced. The drawbacks of knowledge based approaches is that it is tough for a person to remember difficult passwords/PINs; on the contrary easy passwords can be guessed and cracked by intruders. Thus, the authentication system merges token-based and knowledge-based authentication methods, e.g. automated teller machine (ATM) nodes of banks authenticate an individual by taking ATM cards (token) along with a secret PIN (knowledge) as authentication query. However, the combination of knowledge and token based system can not satisfy the security requirements. The primary advantage of biometrics over token based and knowledge based approaches is that, it cannot be misplaced, forgotten or stolen. Also it is very difficult to spoof biometric traits as the person to be authenticated needs to be physically present. A generic biometric system operates by taking an input from the user, preprocessing the signal to denoise it to find the region of interest, extracting features, and authenticating an individual based on the result of comparison [1]. A biometric system has three typical operating modes: enrolment mode, verification mode, identification mode. In enrolment mode, the feature from a subject is extracted and stored in the database. During verification mode, a subject is authenticated by comparing live query biometric template with the database template of the individual whom the subject claims himself to be. The comparison

in this mode is a one-to-one process. In identification mode, the system takes live query template from the subject and searches the entire database to find the best-match template to identify the subject. The comparison in this mode is a one-to-many process.

Various biometric traits like face, iris, fingerprint, gait, voice, face-thermograph, signature are of key research area for many a researchers due to enormous need of security in automated systems. Observing underlying nature of the traits, two basic categories can be identified as: Physiological (or passive) and Behavioral (or active) biometrics [1]. Physiological biometrics are based on direct measurement or data derived from measurement of a part of the human body. A person is identified by his/her face by another person. Fingerprint detection is one of the age-old methods used for recognising the authenticity of a person. However iris pattern, retina tissue pattern, palmprint geometry have evolved as leading physiological biometrics with the evolve of automation of biometric recognition system. Behavioral characteristics, on the other hand, are based on an action taken by a person. Behavioral biometrics, in turn, are based on measurements of data derived from an action, and thereby indirectly measure characteristics of the human body. Voice recognition, keystroke dynamics, and online/offline signature are leading behavioral biometric traits. Suitability of a trait as a biometric for practical implementation is characterised by uniqueness, stability, collectability, acceptability, ease to capture, non-invasiveness and circumvention.

1.1 About Iris Biometrics

Pupil is the darkest circular shaped area in the eye image. Pupil controls the amount of light entering the eye by dilation and contraction. Iris is the circular shaped sphincter that separates pupil from the sclera region. Figure 1.1 depicts the anatomy of human eye on a sample image from CASIAV3 [2] database. As observed, the specular highlights of the acquisition device are made to fall on the pupil region. It is taken care that the highlights do not fall on the iris region as most significant features (viz. freckles, coronas, stripes, furrows, crypts) in the eye image are in the iris. Though the iris region may partially be occluded by eyelids and eyelashes, leading to unconstrained scenario where only partial pattern of iris is available for acquisition. The randomness of the flowery pattern in iris is

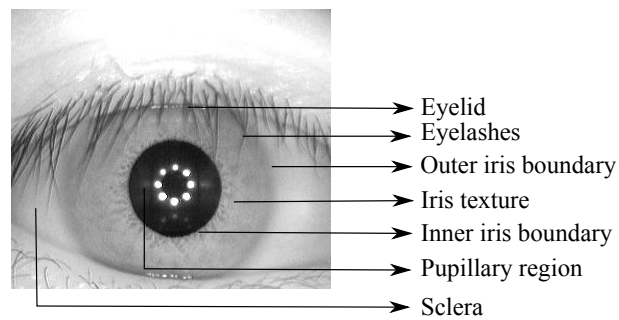


Figure 1.1: An sample image from CASIA database to depict the anatomy of human eye

unique for every individual and hence can work as a token for authenticating an individual. An unimplemented conceptual design of an iris biometric system is first proposed by Drs. Leonard Flom and Aran Safir [3]. The first prototype unit for biometric system was developed in 1995 by L. Flom, A. Safir and J. Daugman. Further researches established iris to be a candidate for reliable and non-cooperative biometric authentication. Iris, due to its permanence and ease of acquiring, plays a significant role among all the biometric traits.

Recent authentication systems need secure, fast and accurate computing for which iris pattern is found to be suitable. Furthermore iris image can be captured without active cooperation of the subject. This marks the suitability of iris recognition also for criminal identification. Iris biometric system involves challenges of automating the system to identify the region of interest, finding useful feature(s) from the region of interest, matching two features when a query comes, maintaining feature sets corresponding to every enrolled subject in the database etc. All these segments are independent research areas and forms an authentication system when deployed together.

1.2 Motivation

Figure 1.2 depicts the block diagram of a generic biometric system constituting conventional phases. As observed from the block diagram, localization is the first phase of iris biometric system. If an iris image is mislocalized, there is no worth of processing it through subsequent phases. And literature survey reveals the fact that there are several issues to be handled for segmenting iris. Firstly, a single static threshold fails to binarize the captured grayscale iris images with varying illuminations. Secondly, iris occlusion by

eyelids and eyelashes degrades the performance of localization module. Thirdly, during image acquisition the spot of light creates specular highlights on pupil which further adds noise to input and hinder the process of localization. Lastly, the gaze of an individual may not be centered in unconstrained situations. Such images are usually acquired in non-cooperative environment. These issues reveal the importance of choosing different binarization thresholds for different images. The minimum value of mean intensity of a grid in iris image has been taken as threshold for binarizing the pupil in [4], but it fails due to specular highlights. Hence the need for hole filling the pupil region is of high importance. Furthermore Daugman's intergradient operator based iris detection suffers from detecting the outer-iris boundary wrongly. Several algorithms are proposed to handle these scenarios where classic algorithms fail. The domain of the first part of the research in this thesis is shown in Figure 1.3. Analytical study of different available algorithms and the detailed elaboration of the proposed research is explored in Section 2.

The second part of the research deals with improvising the performance of matching module. The failure of global feature matching techniques [5] to respond to affine transformation leads to the evolution of local feature matching techniques. Widely used local feature matching techniques like SIFT matches keypoints of one iris image with other on the basis of local descriptor values only. But the descriptor of different regions of iris may be similar. It leads to the fact that matching between two different portions of two different iris images may be done, which is obviously a wrong match. Therefore a necessity of filtering the matched pairs is realised. The intuition of doing so is that false pairs will be pruned, and remaining correct pairs would be able to separate genuine and imposter more accurately. This motivates the second part of the research. The domain of the second part of the research mentioned in this thesis is shown in Figure 1.5 and the elaboration of the concerned research is explored in Section 3.

1.3 Problem Definition

Many a researchers are active in developing robust biometric system as biometric is the latest way of authenticating any individual. However, the biometric system architecture comprises several modules. Current research attempts to make each modules more robust.

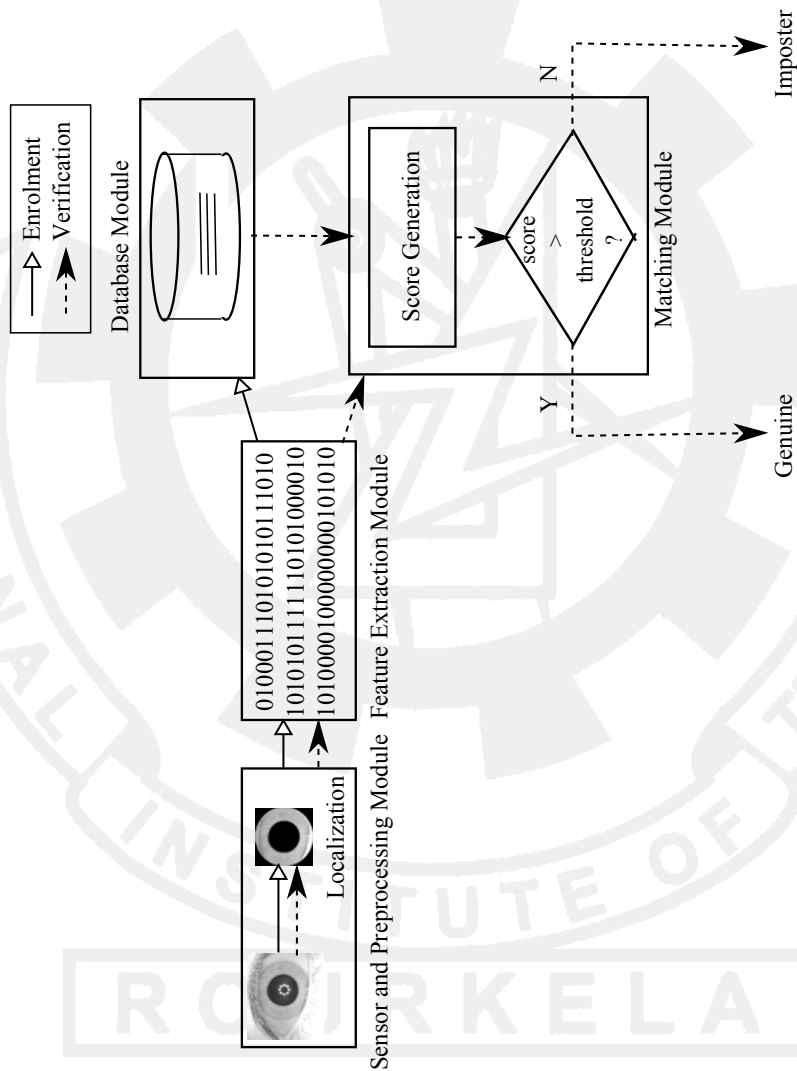


Figure 1.2: Block diagram of generic biometric system

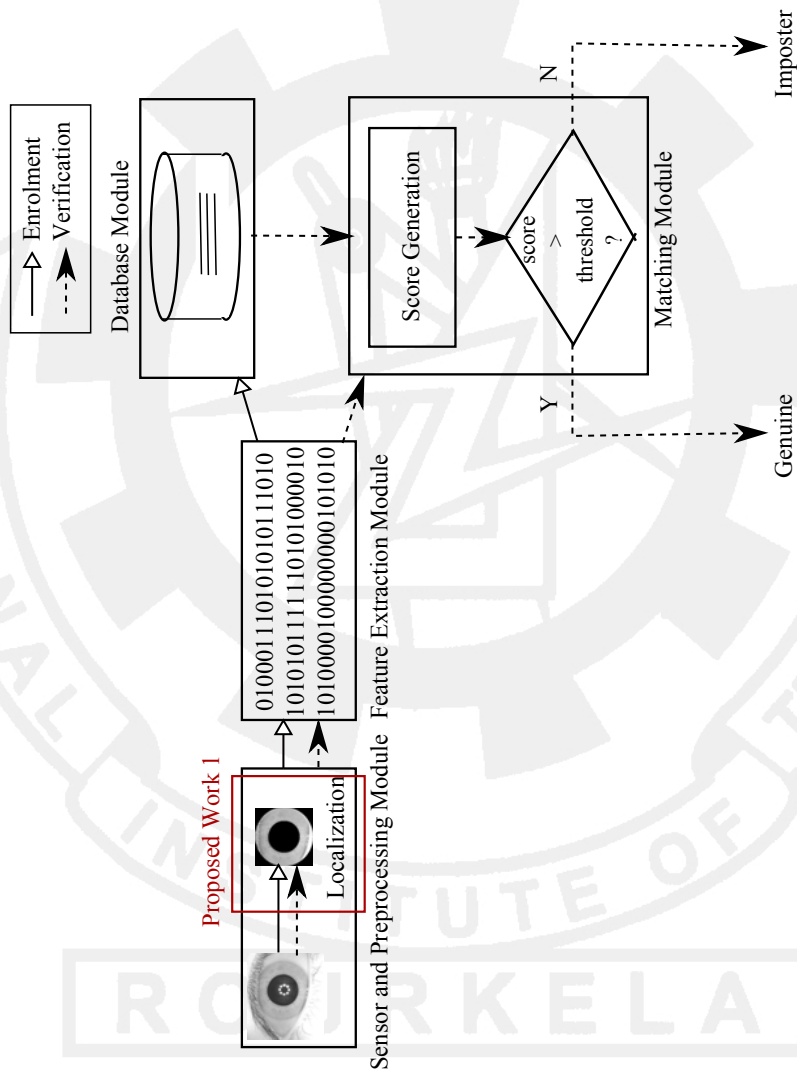


Figure 1.3: Domain of proposed Work I in localization

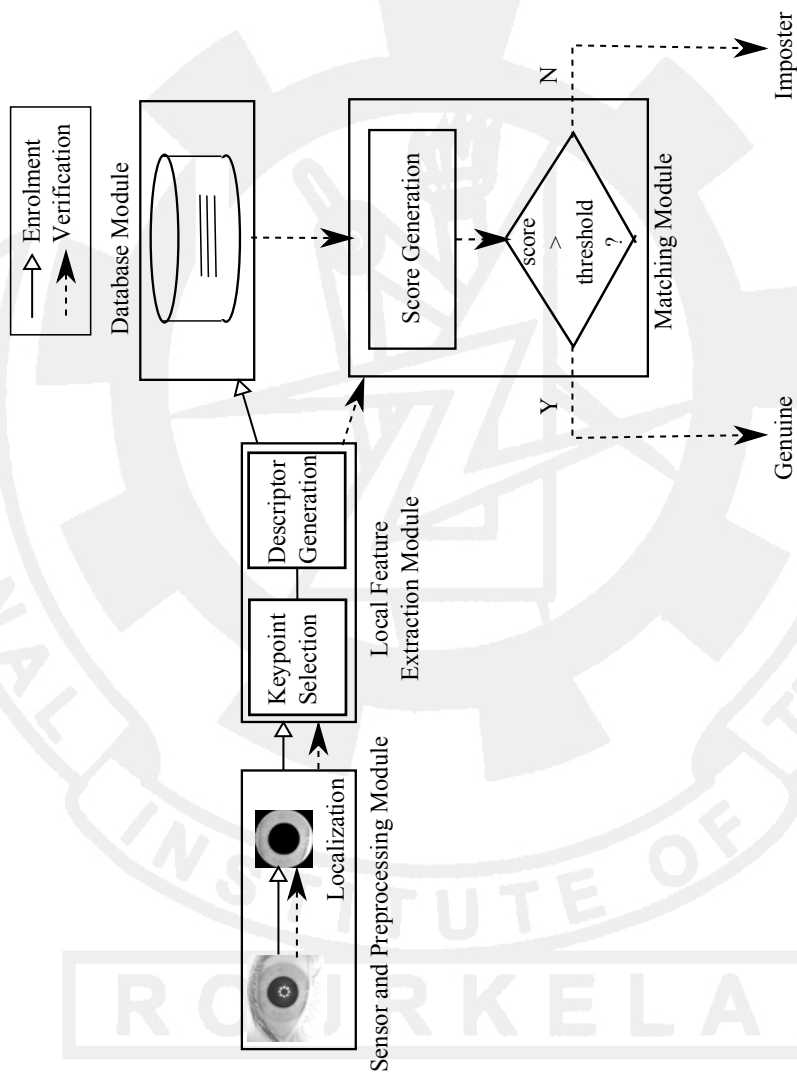


Figure 1.4: Block diagram of local feature extraction based biometric system

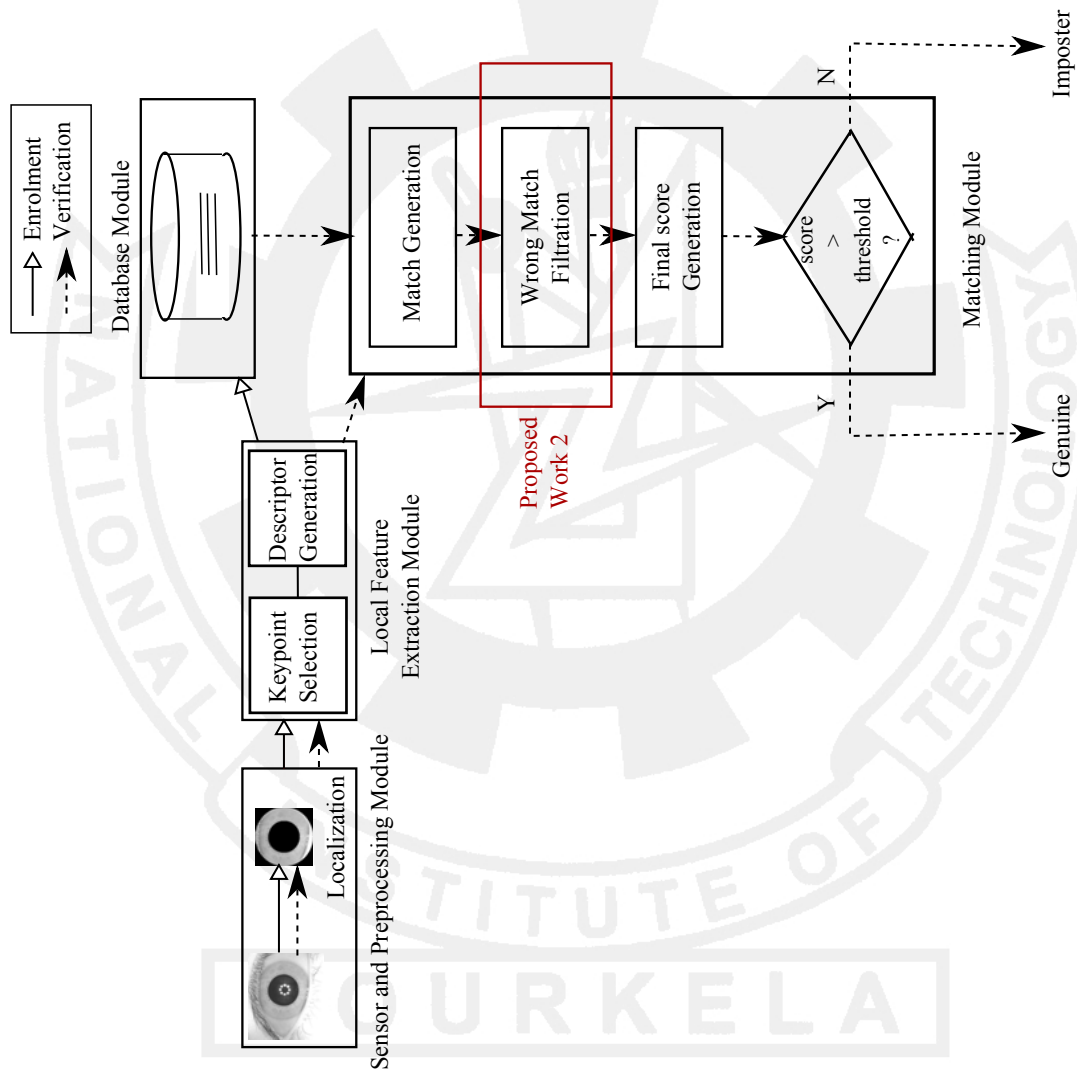


Figure 1.5: Domain of proposed Work II in post matching

Two specific problems are investigated out by the survey of related existing literatures. These issues are addressed and attempted to be resolved in this thesis.

The first problem has two sub-problems: (a) the grayscale threshold choosing problem in binarization during pupil detection, (b) faulty detection of iris radius by integrodifferential operator while outer-iris boundary detection. Both of these sub-problems belongs to localization issues. The first part of the thesis proposes new methods to overcome the studied problems.

The second problem is observed by studying local feature matching schemes like SIFT. A bottleneck of local feature based schemes is that it depends on local feature only for the matching purpose. As it does not take spatial information of keypoints into account, hence it is prone to match two keypoints that are located at different positions of the database and query iris respectively. The second part of the thesis attempts to prune wrong pairs done by SIFT. As a result the proposed approach performs more accurately than the conventional SIFT matching approach.

1.4 Performance Measures Used

The match score generated after testing user given template and database template is deterministic (0:imposter, and 1:genuine) in case of an knowledge based or token based authentication system. It is a process of matching two alphanumeric strings (e.g. password submitted by the subject and corresponding password stored in database). But the matching of biometric templates is more complex due to the reason that n-dimensional biometric templates have no sorted ordering. The second challenge in this domain is that the templates of query and database image do not match exactly due to noise. Hence the matching problem is more of pattern matching. The matching module in the biometric system is responsible for generating a score when a query template and a database template are given as input to it. The generated score is a numerical value signifying how far the query template resembles the database template. Hence the system needs a threshold to decide. Any score below the decided threshold is concluded as an imposter match. Likewise any value above the threshold is concluded as a genuine match. If the threshold is chosen very high, the system would lead some genuine matches to be judged as imposter (False Rejection). On

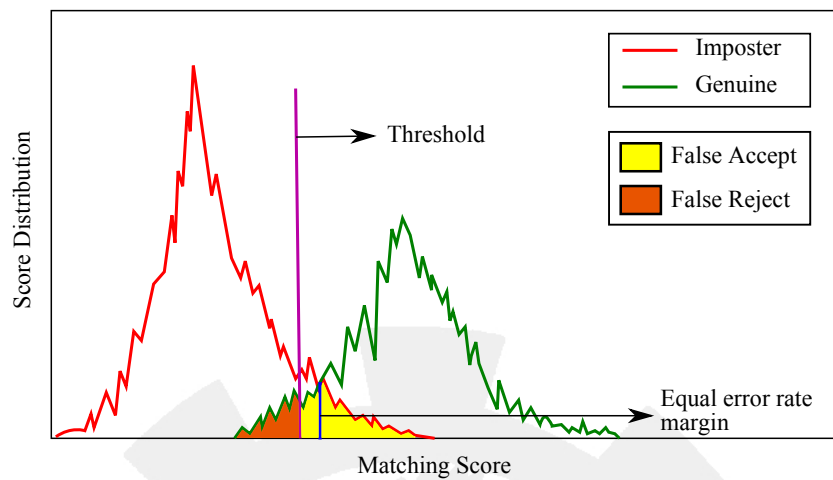


Figure 1.6: Genuine and imposter matching score distribution of biometric database showing various performance measures

the contrary, if the threshold is chosen very low, the system would lead some imposter matches to be judged as genuine (False Acceptance). The choice of threshold value is therefore bears profound significance.

Similarity scores/genuine scores are generated when the two biometric templates of the same subject are compared. This type of score is called genuine-score or intra-class variation. The set of feature chosen should be such that intra-class variation is small. Likewise when two biometric templates of two different subjects are compared, inter-class variation score (imposter-score) is generated. The values of imposter-scores should be high enough to be discriminating from the genuine-scores. However the distribution of genuine-scores and imposter-scores are not mutually exclusive in practical scenarios. Rather they overlap in a certain region. While recognition, the scores that exceed a chosen threshold value (τ), results in false acceptance. The genuine score that falls below τ results in false rejection. Figure 1.6 shows the representation of few performance measures. The commonly used measures to evaluate the performance of biometric systems are:

- **False Acceptance Rate (FAR):** FAR is the frequency of fraudulent access to imposters claiming identity [6]. This statistic is used to measure biometric performance when operating in the verification mode. A false accept occurs when the query template of an individual is incorrectly matched to existing biometric template of another individual.

- **False Rejection Rate (FRR):** FRR is the frequency of rejections relative to people who should be correctly verified. This statistics is used to measure biometric performance when operating in the verification mode. A false reject occurs when an individual is not matched correctly to his/her own existing biometric template.
- **Equal Error Rate (EER):** ERR is the point where FAR is equal to FRR. In general, the lower the equal error rate value, the higher the accuracy of the biometric system. Note, however, that most operational systems are not set to operate at the equal error rate, so the measure's true usefulness is limited to comparing biometric system performance. EER is sometimes referred to as the *Crossover Error Rate*.
- **Genuine Acceptance Rate (GAR):** GAR is the fraction of genuine scores exceeding the threshold τ . It is defined as:

$$GAR = 1 - FRR \quad (1.1)$$

- **Receiver Operating Characteristic (ROC) Curve:** ROC curve depicts the dependence of FRR with GAR for change in the value of threshold. The curve is plotted using linear, logarithmic or semi-logarithmic scales. ROC can also be represented by plotting FRR against FAR for change in the threshold value.
- **Cumulative Match Characteristic (CMC) Curve:** The rank- k identification indicates the number of correct identification that occur in top k matches. Let R_k denote the number of elements of probe set in top k , then the probability of identification is given by $I = R_k/N$. CMC curve represents the probability of identification (I) at various ranks k [7].
- **d-prime Index:** The d' index [1] measures the separation between the arithmetic means of the genuine and imposter probability distribution in standard deviation units is defined as

$$d' = \frac{\sqrt{2} |\mu_{genuine} - \mu_{imposter}|}{\sqrt{\sigma_{genuine}^2 + \sigma_{imposter}^2}} \quad (1.2)$$

where μ and σ are mean and standard deviation of genuine and imposter scores.

- **Rank- k Identification:** The rank- k identification [1] is defined as proportion of times correct identity occurs in top k matches. Cumulative Match Characteristics (CMC) curve plots the ranks against the probability of identification.

1.5 Iris Databases

This section discusses in detail about the databases used in all experiments relevant to the research in this thesis. There exists various available datasets such as UBIRIS version 1 [8], BATH [9], CASIA version 3 [2] and Indian Institute of Technology Kanpur (IITK) [10].

The proposed system has been tested on two publicly available databases, viz. BATH and CASIAV3. Database available from BATH University [9] includes images from 50 subjects. For each subject, images from both the eyes (left and right) each containing 20 images are captured. Database from Chinese Academy of Sciences' Institute of Automation contains 16,213 iris images from 819 eyes acquired in an indoor environment. CASIA version 3 (CASIAV3) [2] is a superset of CASIAV1. In version 3, most of the images have been captured in two sessions with an interval of at least one month. CASIAV3 database comprises 249 subjects with total of 2,655 images from both the eyes.

BATH Database

Database available from BATH University [9] comprises of images from 50 subjects. For each subject, both left and right iris images are obtained, each containing 20 images of the respective eyes.

CASIA version 3 Database

CASIA version 3 (CASIAV3) is acquired in an indoor environment. Most of the images have been captured in two sessions with an interval of atleast one month. The database comprises of 249 subjects with total of 2655 images from left and right eyes. CASIAV3 is a superset of CASIAV1. The pupil regions of all iris images in CASIAV1 were automatically detected and replaced with a circular region of constant intensity to mask out the specular reflections [11].

1.6 Experimental Setup

All experiments relevant to the thesis are carried out on 2.81GHz AMD Athlon 64 X2 Dual Core processor with 2GB RAM. The experiments are simulated using *Matlab*® *Version 7.10.0.499 (R2010a)*.

1.7 Thesis Organization

The entire thesis constitutes three chapters following this chapter. The rest of the thesis is organized as follows:

Chapter 2: Iris localization Using Adaptive Thresholding

This chapter explains an thresholding techniques, edge detection and Circular Hough Transform (CHT) for finding pupil and iris boundary. But CHT requires range of radius as input and is computationally expensive. Proposed localization approach performs faster than the conventional approach. And it works well for change in rotation and change of gaze in iris images and other unconstrained scenarios.

Chapter 3: Postmatch Pruning of SIFT Impairments

This chapter discusses an approach to detect false pairs that SIFT generates because of texture similarity of several keypoints from different regions of iris image. The chapter proposes two techniques of filtering wrong keypoints, viz. angular filtering and scale filtering. Experimental results justify that the proposed postmatch filtration of approach to devise an adaptive threshold of binarization for pupil detection and a canny detected edge map based iris detection. Many researchers have used variations of impairments improves accuracy of recognition.

Chapter 4: Conclusions and Future Work

This chapter presents analytical remarks to overall achievements and limitations of all the proposed works, concluding with scope for further research work in this domain.

Chapter 2

Iris localization Using Adaptive Thresholding

Conventional 2-D image acquisition systems also capture immediate surroundings of eye region while capturing iris [12]. Primarily it is significant to segment the portion of the image containing exclusively iris. Specifically, it is important to localise the region between inner pupil and outer iris boundary. If iris is occluded by eyelids (which happens in most of the cases for unconstrained data) then portion between the upper and lower eyelids should only be considered for the extraction of local features. Further, there may exist some specular highlights on pupil region. Preprocessing is an important step which involves the method of converting a crude acquired input image into only region of interest, from which feature extraction can be done. The conventional steps involved in iris image preprocessing are: (i) to remove specular highlights on the pupillary area via hole-filling operation, (ii) to localise the inner and outer iris boundaries (often modelled by two best fitted concentric circles or ellipses), (iii) to remove eyelids and eyelashes which hinder feature extraction process and (iv) to transform the annular iris into a rectangular block using Cartesian to polar conversion. However, H. Proenca and L.A. Alexandre points out in [13] that the texture features are distorted or partially lost due to aliasing during polar transformation [as mentioned in Step (iv) above]. Hence, in the proposed research eyelid removed annular region is considered directly for the purpose of feature extraction. This chapter discusses literature survey on iris localization and proposed iris localization schemes in sequence.

The proposed approaches are compared with existing conventional detection techniques.

2.1 Literature Survey

Significant amount of work has been done for iris segmentation in the last decade. J. Daugman has used integrodifferential operator for iris localization [14] but the location of iris varies from image to image; so global search reduces speed. Wildes has used edge detection and circular Hough transform [12] together for the purpose. In order to improve localization time, coarse to fine strategy is proposed by Huang et. al [15]. In the coarse stage, the technique finds outer iris boundary in the re-scaled image, then using that information iris circles are found using integrodifferential operator. There are various approaches developed as an improvement over traditional Hough transform. In [16], the authors have used Canny edge detector with Hough transform to improve localization speed. By means of canny edges, normal line algorithm is created for finding center and inner edge. Homocentric circle algorithm is used to find outer edge. The authors in [17] have used bisection method to find inner boundary. Further, histogram equalisation and statistical information is used to find collarete boundary. In addition to this, the authors in [18] provided an improvement over Hough transform for circle to restrict votes for center location based on direction of edges. The algorithm proposed in [19] is used to overcome the drawback of traditional iris localization approaches that are affected by eyelid occlusion and are time consuming. In the coarse localization of inner boundary, the lower contour of pupil is used for estimation of parameters. In coarse localization of outer boundary the average intensity signals on both sides of pupil are used to estimate the parameters. In fine stage, Hough transform is used to localise boundaries precisely. Table 2.1 (taken from [5]) evinces some benchmark approaches (placed in chronological ordering) along with respective performance measures.

Some authors have used thresholding based approaches to find coarse localization of pupil. The authors in [27] search for pixels below a threshold as pupil and then use Hough transform and edge detection to find circles in the limited area. Further, an automatic iris segmentation based on local areas is proposed in [4]. In this approach, iris image is divided into rectangular grid and mean is obtained for each block. The minimum value of mean

Table 2.1: Performance comparison of some benchmark localization approaches

Year	Authors	Approach	Testing Database	Accuracy Results
2002	Camus et al.[20]	Multi-resolution coarse-to-fine strategy	Constrained iris images (640 without glasses, 30 with glasses)	overall 98% (99.5% for subjects without glasses and 66.6% for subjects wearing glasses)
2004	Sung et al.[17]	Bisection method, canny edge-map detector and histogram equalization	3,176 images acquired through a CCD camera	100% inner boundary and 94.5% for collarette boundary
2004	Bonney et al.[21]	Least significant bit plane and standard deviations	108 images from CASIA v1 and 104 images from UNSA	Pupil detection 99.1% and limbic detection 66.5%
2005	Liu et al.[18]	Modification to Masek's segmentation algorithm	317 gallery & 4,249 probe images acquired using Iridian LG 2200 iris imaging system	97.08% Rank-1 recognition
2006	Proenca et al.[22]	Moment functions dependent on fuzzy clustering	1,214 good quality images, 663 noisy images acquired from 241 subjects in two distinct sessions	98.02% on good data set and 97.88% on noisy data set
2008	Pundlik et al.[23]	Markov random field and graph cut based energy minimization	WVU Non-ideal database	Pixel label error rate 5.9%
2009	He et al.[24]	Adaboost-cascade iris detector for iris center prediction	NIST Iris Challenge Evaluation (ICE) v 1.0, CASIA-Iris-V3-lamp, UBIRISv1.0	0.53% EER for ICEv1.0 and 0.75% EER for CASIA Iris-V3-lamp
2010	Jin et al.[25]	K-means cluster	CASIAv3 and UBIRISv2.0	1.9% False Positive and 21.3% False Negative (on a fresh data set not used to tune the system)
2010	Tan et al.[26]	Gray distribution features and gray projection	CASIAv1	99.14% accuracy with processing time of 0.484second/image

is taken as threshold for binarizing the pupil as shown in Figure 2.1 [4]. Some work has been proposed in the direction of non-cooperative iris localization. The authors in [22] have implemented the segmentation methodology proposed by Tuceryan [28] used the moments in small windows of the image as texture features and then applied a clustering algorithm to segment the image. Further a robust segmentation approach for non-ideal images has been developed using graph cuts [23].

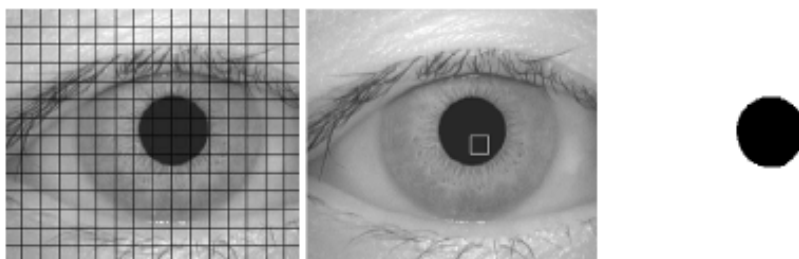


Figure 2.1: Grid based binarization using adaptive threshold

There are several issues that have been observed from the literature. Firstly, static threshold fails to binarize iris image for varying illumination. Secondly, iris is occluded by eyelids and eyelashes. This further degrades the performance of localization module. Thirdly, during image acquisition the spot of light is made to fall on the pupil region. This creates specular highlights which in turn adds noise to the input image. Lastly, the gaze of an individual may not be centered. Such images are usually acquired in non-cooperative environment where little or no restriction is imposed upon the subject during acquisition. In the proposed work, a robust iris segmentation approach has been developed that performs well for aforementioned non-cooperative data sets. The proposed scheme is based on adaptive thresholding. The details of the approach is discussed in Section 2.2. The hole filled binary image is used for finding pupil boundary using spectrum image (Section 2.3). Section 2.4 outlines the approach to find outer iris boundary. Experimental results for the proposed approach are given in Section 2.5.

2.2 Proposed Adaptive Thresholding

Pupil is the darkest region in the eye with almost circular shape. Appropriate threshold helps in finding the region of interest that contains pupil. Static value of threshold may

fail for different images taken under varying illumination conditions [4]. Thus, in the proposed research an effort has been made to adaptively determine the value of threshold. It has been empirically found that the highest intensity value contributing to pupil neither exceeds $high_\tau$ (0.5 of highest grayscale value) nor drops beyond low_τ (0.1 of highest grayscale value). To find adaptive threshold, binary images are obtained iteratively for range of thresholds (τ) between low_τ and $high_\tau$ with an increment of $step_\tau$ (0.05 of highest grayscale value). Choosing a low value of $step_\tau$ would force the system to generate more number of binary images, and hence increasing execution time. Likewise, choosing a high value of $step_\tau$ would generate less number of binary images and hence may miss out the appropriate binarization threshold. These parameters are optimized based on trade off between computational complexity and performance accuracy.

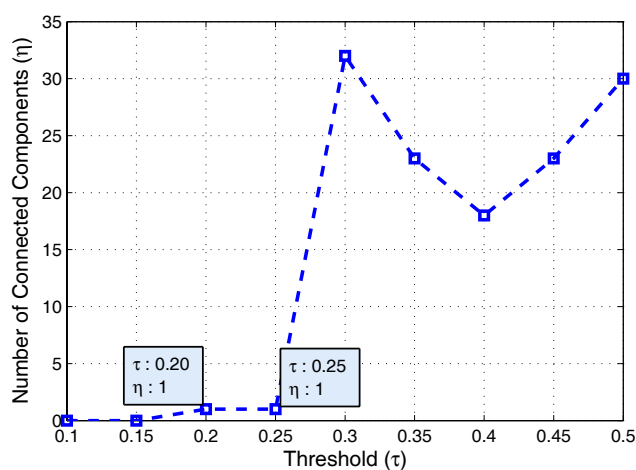


Figure 2.2: Relationship between τ and η

The binary images obtained for varying τ are considered for removing specular highlights (holes). These highlights add noise and hinder pupil segmentation process. The holes are required to be detected and filled because pupil localization works more efficiently for completely filled circle. Morphological region filling approach is used to fill holes in the image [29]. To begin with hole filling operation, binary image (A) is complemented. The convention adopted here is that the boundary pixels are labelled as 1. If non-boundary pixels are labelled as 0 then beginning with a point p inside the boundary, a value of 1 is

assigned. The following transformation fills the region with ones.

$$X_k = (X_{k-1} \oplus S) \cap A^c \quad (2.1)$$

where $X_0 = p$; $k = 1, 2, 3, \dots$; \oplus is used for dilation of X_{k-1} by S which is defined as

$$X_{k-1} \oplus S = \{z | (\hat{S})_z \cap X_{k-1} \neq \phi\} \quad (2.2)$$

The symmetric structuring element S is defined as,

$$S = \begin{bmatrix} 0 & 1 & 0 \\ 1 & 1 & 1 \\ 0 & 1 & 0 \end{bmatrix}$$

This algorithm terminates at k^{th} iteration, if $X_k = X_{k-1}$. The image generated from last iteration X_k is combined with A using bitwise OR that contains the boundary filled image.

Each hole filled image is used for finding the number of connected components (η) [29]. η changes for change in value of threshold as shown in Figure 2.2. The value of threshold corresponding to minimum non-zero η is chosen as adaptive threshold for binarization. However, if the minimum non-zero η occurs for more than one thresholds (as shown in Figure 2.2), then maximum threshold amongst them is chosen as adaptive threshold. The reason behind finding maximum amongst potential thresholds is that pupil boundary may contain some intensity values which may not contribute to connected component of pupil for lower thresholds. Figure 2.3 shows the binary images obtained for change in τ . Algorithm 2.1 describes the steps involved in finding the non-noisy binary image.

2.3 Pupil Detection

In traditional iris recognition systems, combination of edge detection and Circular Hough Transformation (CHT) is used for finding pupil and iris boundaries [27]. The major drawback of Hough transform is that it requires range of radius as input from the user. Further, Hough works in R^3 parameter space (number of parameters needed to describe the

Algorithm 2.1 Proposed_Adaptive_Thresholding**Input:** I : Intensity Image, S : Structuring element**Output:** B : Binary Image

```

1:  $low_\tau \leftarrow 0.10$ 
2:  $high_\tau \leftarrow 0.50$ 
3:  $step_\tau \leftarrow 0.05$ 
4:  $[r\ c] := \text{size}(I)$  {Compute width and height of image}
5: for  $\tau := low_\tau$  to  $high_\tau$  step  $step_\tau$  do
6:    $A := \text{binary}(I, \tau)$  {Image Binarisation using  $\tau$ }
7:    $C := A^c$  {Complement of an image}
8:    $X_0 := \text{zeros}(r, c)$  {Image with all zeros}
9:    $X_0(p) = 1$  { $p$  is a point inside hole}
10:   $k \leftarrow 0$ 
11:  repeat
12:     $k \leftarrow k + 1$ 
13:     $X_k \leftarrow (X_{k-1} \oplus S) \cap C$ 
14:  until  $X_k \neq X_{k-1}$ 
15:   $H_\tau \leftarrow X_k \cup A$  {Hole filled image}
16:   $\eta_\tau := \text{connComp}(H_\tau)$  {Find number of connected components (Insignificantly small
    sized components are not taken into account)}
17: end for
18:  $pos := \text{min\_nonzero}(\eta)$  {Find index of minimum non-zero}
19:  $B \leftarrow H_{pos}$ 
20: return  $B$ 

```

shape of a circle) which in turn increases the time complexity of the transform. Hence, an efficient spectrum based approach is used for pupil detection that performs faster compared to Hough transformation without any priori estimation of radius.

In this approach, the binarised image is re-complemented to detect center of pupil. The distance of every pixel in the binary image is obtained with nearest non-zero pixel [30]. By computing the distance between pixels, spectrum showing largest filled circle can be formed within the set of foreground pixels. Since pupil is the largest filled circle in the image, the overall intensity of this spectrum is maximum at the center. The spectrum image is shown in Figure 2.4(a). Thus, the position of maximum value in the spectrum image is pupil center. To compute the pupil radius, an edge map of the hole filled binary image is obtained as shown in Figure 2.4(b). In the edge map, the distance from the detected pupil

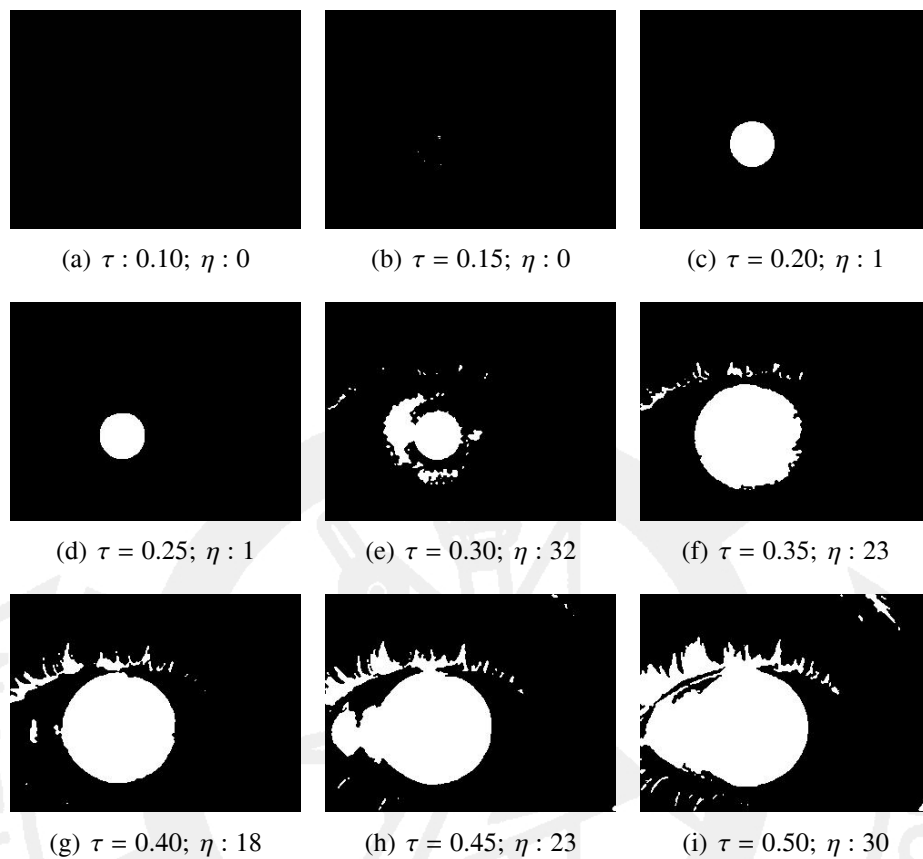


Figure 2.3: Binary images obtained for change in threshold (τ) and number of connected components (η)

center to the nearest non-zero pixel is the pupil radius (r_p). The pupil detected image is shown in Figure 2.4(c). The algorithm for detecting pupil center and radius is given in Algorithm 2.2.

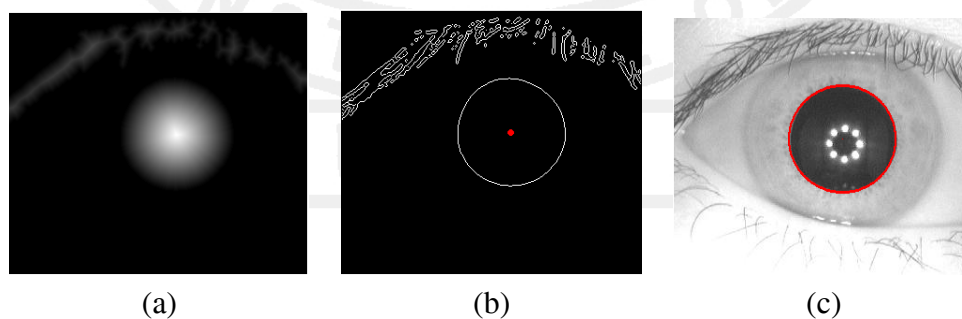


Figure 2.4: Pupil Detection: (a) Spectrum image, (b) Edge detected image with pupil center and (c) Pupil localised image

Algorithm 2.2 Pupil_Detection**Input:** B : Binary Image**Output:** x_c : xcenter of pupil, y_c : ycenter of pupil, r_p : Radius of pupil

```

1:  $C \leftarrow B^c$  {Complement the binary image}
2:  $[x \ y] := \text{find}(C == 1)$  {Find location of ones in an image}
3:  $l := \text{length}(x)$  {To find the number of elements in an array}
4: for  $i := 1$  to  $r$  do
5:   for  $j := 1$  to  $c$  do
6:     for  $k := 1$  to  $l$  do
7:        $D_k \leftarrow \sqrt{(x_k - i)^2 + (y_k - j)^2}$ 
8:     end for
9:      $S_{i,j} := \min(D)$  {Minimum value of  $D$ }
10:  end for
11: end for
12:  $[x_c \ y_c] \leftarrow \max(S)$ 
13:  $E := \text{edge}(C)$  {Edge detection [29]}
14:  $j \leftarrow y_c$  {Estimation of pupil radius}
15:  $r_p \leftarrow 0$ 
16: while  $E_{x_c,j} \neq 1$  do
17:    $r_p \leftarrow r_p + 1$ 
18:    $j \leftarrow j + 1$ 
19: end while
20: return  $x_c, y_c, r_p$ 

```

2.4 Iris Detection

For iris detection, the intensity image is blurred to remove external noise. But too much blurring may make it difficult to detect the outer iris boundary, separating the eyeball and sclera. Thus, a special smoothing filter such as the median filter is used on the original intensity image. This type of filtering eliminates sparse noise while preserving image boundaries [29]. After filtering, the contrast of image is enhanced to have sharp variation at image boundaries using histogram equalisation as shown in Figure 2.5 (a).

This contrast enhanced image is used for finding the outer iris boundary by drawing concentric circles (Figure 2.5 (b) shows an example) of different radii from the pupil center and the intensities lying over the perimeter of the circle are summed up [31]. Among the candidate iris circles, the circle having maximum change in intensity with respect to the

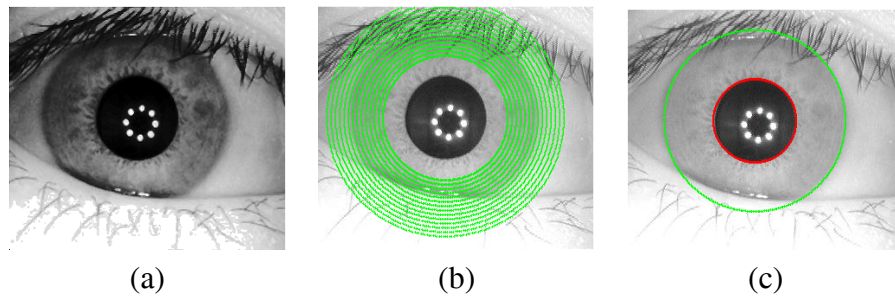


Figure 2.5: Iris Detection: (a) Contrast enhanced image (b) Concentric circles of different radii (c) Iris localised image

previous drawn circle is the iris outer boundary as shown in Figure 2.5 (c). The algorithm for detection of iris radius (r_i) is given in Algorithm 2.3.

Algorithm 2.3 Conventional_Iris_Detection

Input: I : Input image, r_p : Radius of pupil, x_c : xcenter of pupil, y_c : ycenter of pupil

Output: r_i : Radius of iris

```

1:  $F \leftarrow \text{medianFilt}(I)$  {Median Filtering on input image}
2:  $H \leftarrow \text{Histeq}(F)$  {Histogram equalisation}
3:  $[r \ c] \leftarrow \text{size}(I)$  {Finding image dimensions}
   {Finding the intensity over circumference}
4: for  $r_i = r_p \times 1.5$  to  $\frac{r}{2}$  do
5:    $\text{sum}_{r_i} \leftarrow 0$ 
6:   for  $\theta = 0$  to 360 do
7:      $x = x_c + r_i \times \cos(\theta)$ 
8:      $y = y_c + r_i \times \sin(\theta)$ 
9:      $\text{sum}_{r_i} = \text{sum}_{r_i} + H_{x,y}$ 
10:  end for
11:   $r_i = r_i + 2$ 
12: end for
   {Change in intensity over circumference}
13: for  $i = 1$  to  $r_i$  do
14:   $D_i = |\text{sum}_i - \text{sum}_{i+1}|$ 
15: end for
16:  $[d \ r_i] = \max(D)$  {Maximum change in intensity}
17: return  $r_i$ 

```

This approach fails sometimes due to high texture pattern in the iris region. This method deduces iris boundary much prior to actual boundary is reached as shown in Figure 2.6. To

alleviate this problem, we propose a novel iris detection scheme which is discussed below in details.

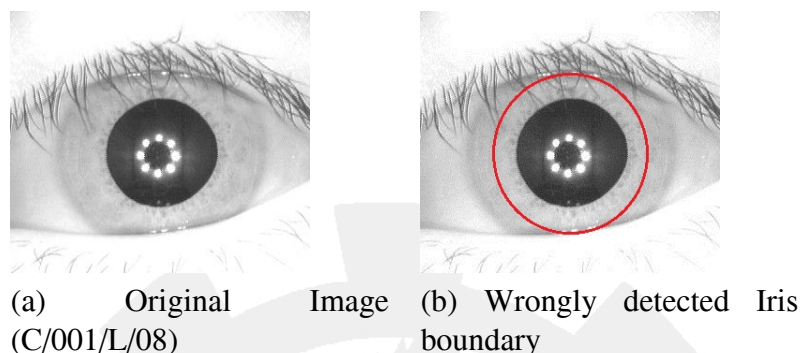


Figure 2.6: Classic Integrodifferential operator applied over median-filtered intensity image fails to detect iris boundary

2.4.1 Proposed Iris Detection

To overcome the problem in Section 2.4, an alternative approach has been used to suppress the iris textures before applying the classic operation. Canny edge detector when applied to an iris image preserves strong edges corresponding to iris boundary but mostly suppresses edges due to textures within iris. Hence the proposed approach uses circular summation integrodifferential operator on canny detected edge image to find the iris boundary.

Starting from a radius just more than the pupil boundary, concentric circles are drawn and number of edge pixels falling upon each circle is counted. The process goes until the testing circle has a radius thrice of the radius of the pupil. The circle on which maximum number of edge pixels are found is inferred to be the best fitted circle over iris boundary. The details of the steps are given in Algorithm 2.4. The steps and output of the stated algorithm are depicted in Figure 2.7.

To decrease the execution time of this algorithm, r_{low} and r_{high} can be chosen more intelligently depending on the knowledge of human eye anatomy. In the implementation, rather than taking r_{low} to be $(r_p + \delta)$, it can be taken as $(1.5 \times r_p)$, based on the fact that width of iris is at least half of the pupil radius. The proposed pupil and iris segmentation method applied together works well for human iris and efficiently segments region of interest for further biometric processing.

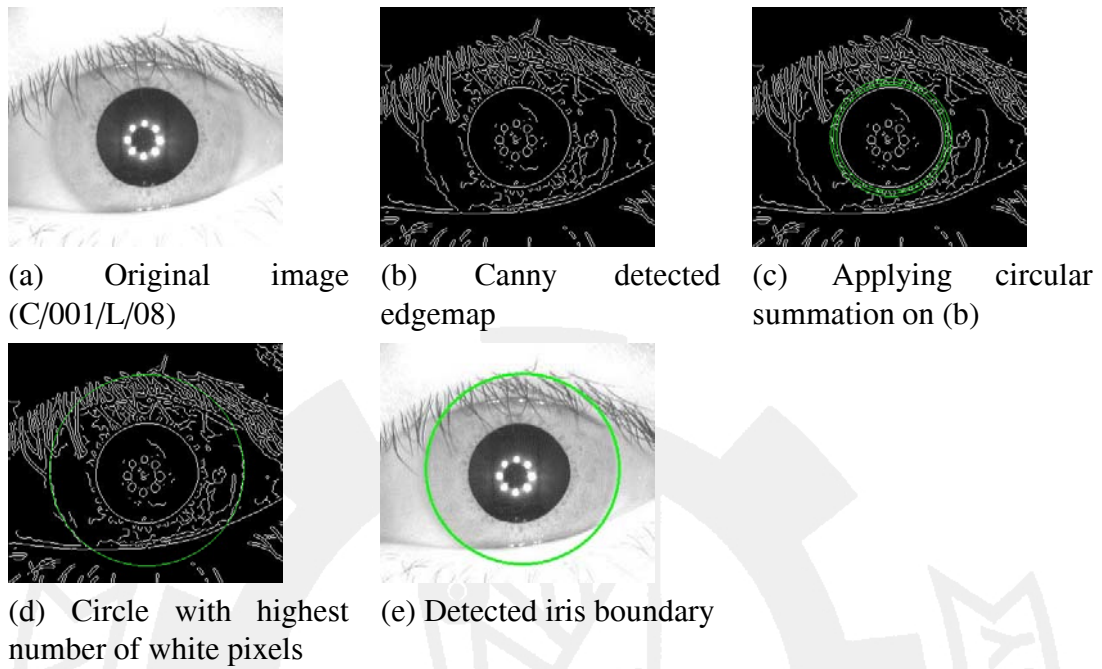


Figure 2.7: Modified intergradient operator applied over canny edge detected image detects iris boundary

Algorithm 2.4 Proposed_Iris_Detection

Input: I : Input image, r_p : Radius of pupil, x_c : xcenter of pupil, y_c : ycenter of pupil

Output: r_i : Radius of iris

- 1: $BW \leftarrow \text{cannyEdge}(I)$ {Edge detection using Canny Detector}
 - 2: $r_{low} \leftarrow r_p + \delta$ {Search of iris radius begins from a value just more than pupil center}
 - 3: $r_{high} \leftarrow 3 \times r_p$ {Search of iris radius ends at a value just more than pupil center}
 - {Finding number of edge (white) pixels over circumference}
 - 4: **for** $r_i = r_{low}$ to $3 \times r_{high}$ **do**
 - 5: $count_{r_i} \leftarrow 0$
 - 6: **for** $\theta = 0$ to 360 **do**
 - 7: $x = x_c + r_i \times \cos(\theta)$
 - 8: $y = y_c + r_i \times \sin(\theta)$
 - 9: $sum_{r_i} = sum_{r_i} + BW_{x,y}$ {If $BW_{x,y}$ is 1 (white), then the value of sum_{r_i} is incremented}
 - 10: **end for**
 - 11: **end for**
 - {Finding maximum number of white pixels}
 - 12: $[d r_i] = \max(sum)$
 - 13: **return** r_i
-

2.5 Experimental Results

The proposed algorithm is run on all images of BATH and CASIAV3 databases. From experimental analysis it has been observed that the system is capable of handling unconstrained scenarios as well. To mention a few, it possesses invariance to noisy instances viz. occlusion, specular highlights, person wearing contact lens, change in illumination and viewpoint (non-centered gaze). Performance accuracy of the detector is supported with the help of few illustrations. The nomenclature of the images are defined as *Database/Subject ID/Eye/Image Instance* (e.g. C/224/L/05).

Figure 2.8 (a) depicts the robustness against occlusion and specular highlights. It is evident that the proposed scheme performs well for higher degree of occlusion (C/010/R/04) where image is occluded by upper eyelid and the region of interest (iris) is partially outside. Further, an example showing the subject wearing contact lens is shown in Figure 2.8 (b). The segmentation takes place accurately despite unconstrained nature of the instances.

Similarly, the system is proficient in performing against illumination variation. The

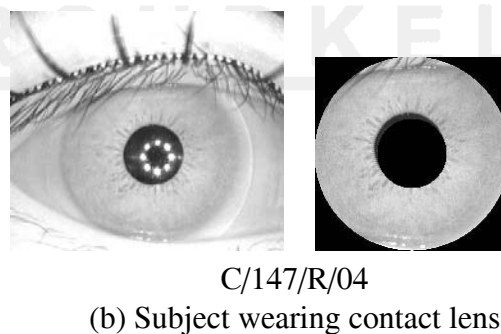
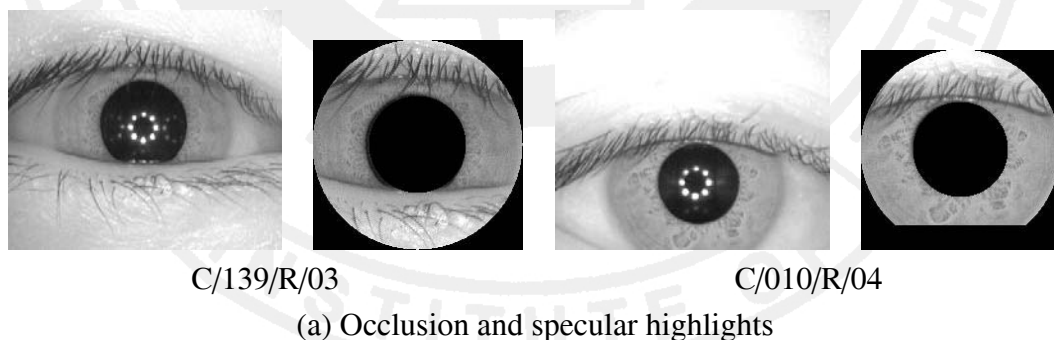


Figure 2.8: Localization performance of the proposed approach for (a) occlusion and specular highlights and (b) contact lens

change in illumination leads to dilation and contraction of pupil. Static threshold may fail to perform as intensity variation occurs due to illumination. Few such samples from BATH and CASIAV3 databases are shown in Figure 2.9.

Table 2.2: Accuracy (in %) for the proposed approach and Hough transform

Databases → Approach ↓	BATH	CASIAV3
Hough	99.53	95.17
Proposed	99.07	95.76

The localization accuracy of the proposed system is compared against circular Hough transform [12] as shown in Table 2.2. The proposed system performs with an accuracy of 99.07% and 95.76% on BATH and CASIAV3 respectively (with an average accuracy of 97.42%). Hough transform performs equally well (average accuracy of 97.35%) but localization time for the proposed system is relatively low compared to conventional Hough transform.

Few test cases where proposed approach outperforms Hough transformation are shown in Figure 2.10. In order to determine computation efficiency, time taken to perform

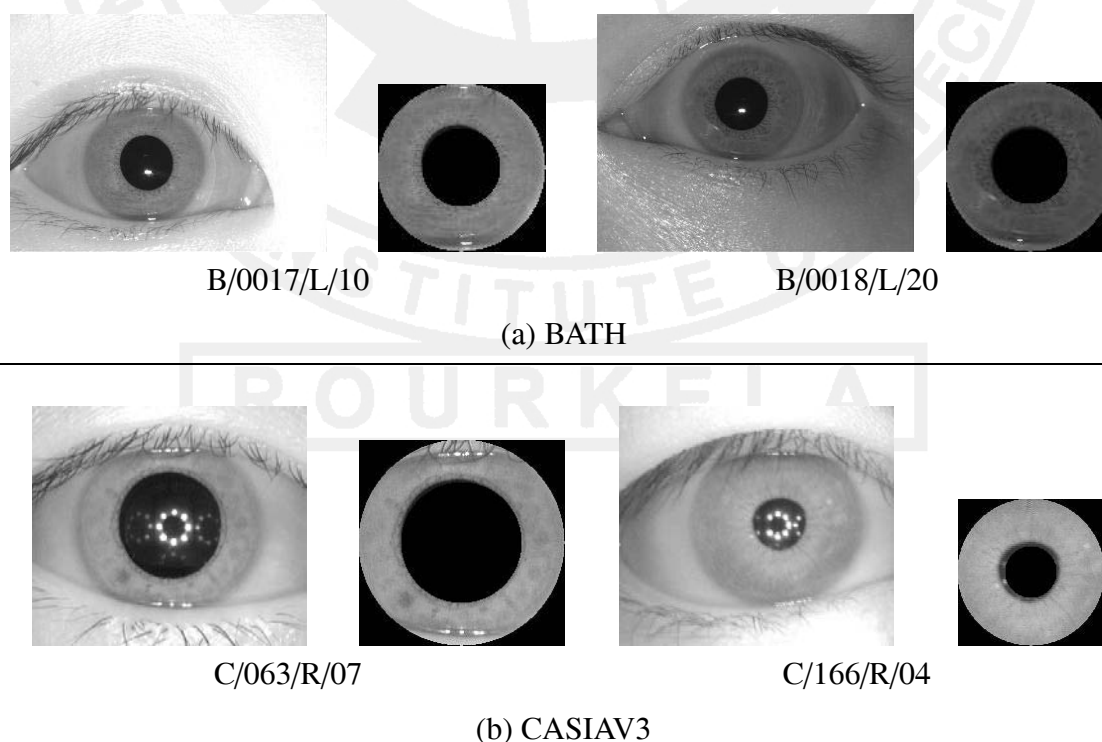


Figure 2.9: Localization performance of the proposed system for variation in illumination

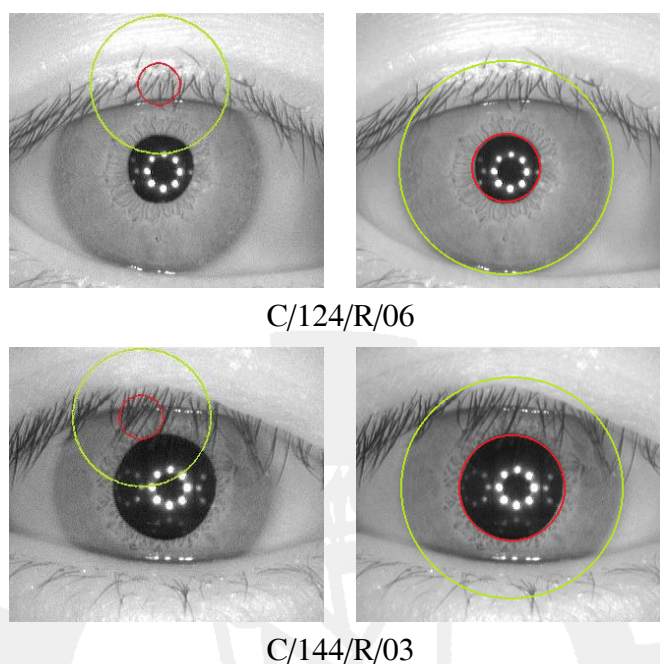


Figure 2.10: Sample instances where proposed approach (right) performs better than Hough transform (left)

segmentation is computed.

Time required to perform localization by the proposed approach is significantly low compared to Hough transform as given in Table 2.3. Average time taken by the proposed approach is 0.37 seconds/image whereas Hough takes 7.68 seconds/image.

Table 2.3: Time taken (in seconds) for the proposed approach and Hough transform

Databases → Approach ↓	BATH	CASIAV3
Hough	02.2820	13.0676
Proposed	00.3383	00.3960

2.6 Summary

From the results it is evident that the system is capable of performing segmentation for unconstrained scenarios in significantly less time. The results are compared against benchmark localization approach (Hough transform). From the experiments it has been observed that the proposed approach performs with an average accuracy of 97.42% in comparison to Hough which performs with an average accuracy of 97.35%. Though there

is minor improvement in accuracy, the time required to perform segmentation significantly reduces to 0.37 seconds/image in comparison to 7.68 seconds/image for Hough transform. This marks the suitability of the proposed approach over traditional high complexity Hough transform for time constrained systems.



Chapter 3

Postmatch Pruning of SIFT

Impairments

There has been significant research done in the area of iris recognition using global features [5]. However, these approaches fail to possess invariance to change in scaling, rotation, occlusion, illumination and viewpoint between database and query iris image. The current research is mainly focussed on iris images taken under unconstrained environment [32]. Thus, there is stringent requirement to develop iris recognition system suitable for non-cooperative images. Keypoint descriptors are invariant to affine transformation as well as partial occlusion. Matching two iris images using local features is challenging when applied to iris. Each keypoint in gallery iris image is paired to corresponding keypoint in probe iris image using nearest neighbor approach [33]. Matching only using feature descriptor may wrongly pair keypoints that are not from same iris region rather share similar descriptor information. Thus, matching algorithm should be designed considering both spatial and descriptor properties of a keypoint. The challenge with conventional SIFT matching when applied to iris recognition is to eliminate noisy pairs.

In this chapter an effort has been made to combine spatial and descriptor information of keypoints for finding accurate pairs. The keypoints paired using SIFT are taken into consideration to perform post filtering operation. Post filtering of keypoints is an elimination process where wrong pairs are selected and removed hierarchically. In the

first stage, the gradient information of keypoints is obtained with respect to iris center. The pairs that fall outside the angular tolerance are selected and removed. From the candidate pairs obtained after gradient filtering, scale based filtering is performed by finding the ratio of local keypoint scaling with respect to center to global scaling factor. The pairs that lie outside the scale range are further eliminated to finally obtain potential pairs. This pruning approach has been particularly applied to iris and it is experimentally observed that it improves the performance of unconstrained iris recognition system using local features. This rest of the section is organized as follows. The existing review for iris recognition is given in Section 3.1. Section 3.2 explains feature extraction and matching using traditional SIFT approach. The proposed approach for angular and scale filtering is presented in Section 3.3. Experimental results for the proposed approach and its comparison with SIFT is presented in Section 3.4. Finally, conclusions are given at the end of the chapter.

3.1 Related Works

Daugman has developed an operational iris biometric system and is successful in finding its deployment for entry into United Arab Emirates (UAE) [14, 34]. The authors in [5] have presented a survey over various iris recognition systems reported in literature. In [35] Gaussian filter is used for texture representation. The gradient vector field of an iris image is convolved with a Gaussian filter, yielding a local orientation at each pixel from normalised iris image. Dyadic wavelet transform of a sequence of 1-D intensity signals around the inner part of the iris has been used in [31] to create a binary iris code. The system achieves 0.07% of EER. In [36] modified Log-Gabor filters are used because Log-Gabor filters are strictly band pass filters but Gabor filters are not. Discrete Cosine Transform (DCT) is used for feature extraction in [37]. DCT is applied to rectangular patches rotated at 45 degrees from radial axis. The dimensionality of feature set is reduced by keeping three most discriminating binarized DCT coefficients. The authors in [38] have done texture analysis by computing the analytic image. The analytic image is the sum of the original image signal and Hilbert transform of the original signal. The approaches mentioned in the literature performs well when the data is cooperative with centered gaze. Further, it is important to transform iris into polar plain for performing recognition. The transformation

of iris from Cartesian to polar coordinates creates aliasing effect [13].

There has been some advancement done for iris recognition using non-cooperative images. The keypoint descriptors are capable of performing recognition under change in transformation, occlusion and illumination. These features are detected directly from annular iris image without any transformation from Cartesian to polar plane. Scale Invariant Feature Transform (SIFT) is a well known keypoint descriptor for object recognition [33]. Due to inherent advantages, SIFT is capable of performing recognition using non-cooperative iris images [39]. Iris features are extracted without polar transformation and feature point descriptors are transformation, illumination and occlusion invariant. The authors have performed matching for each major region: left, right, and bottom independently. Prompted by the performance of SIFT, authors in [40] have applied Speeded Up Robust Features (SURF) [41] on sectorized iris image for recognition. From experimental results it has been observed that SURF based local descriptor performs better than its Harris and SIFT similitudes.

However, the major challenge is to find exact pairs between keypoints from gallery and probe iris images. Lowe [33] has found the pairs by using nearest neighbour search. The best pair for every keypoint in gallery image is found by identifying the nearest neighbor from query image. Nearest neighbor is defined as keypoint with minimum Euclidean distance for affine invariant descriptor vector. There may be features which may not have good matches and should be discarded. A global threshold in such cases may fail as some descriptors may be more discriminating than others [33].

A more effective approach adapted is to compare the distance of closest neighbor to that of second closest neighbor. This yields more reliable matches compared to primitive distance based approach. Matching approach demands to find distance between each keypoint of query image to each keypoint of database image. So the nearest neighbor matching approach bears $O(pq)$ complexity where p and q denotes number of detected keypoints in query and database images respectively. In order to improvise the speed of SIFT matching, kd-trees are used [42]. A kd-tree is a binary tree in which every node is a k-dimensional point that generates a hyperplane that divides spaces into two subspaces. Points to the left are represented as left sub-tree and points to the right are

represented by right sub-tree. This approach works well for low dimensional data but loses its effectiveness as the dimensionality increases. To speed up search by finding approximate nearest neighbor, multiple randomized trees are created as proposed in [43]. The authors in [44] have improved kd-tree's search performance by creating multiple trees from same data and simultaneously searching among the trees. Further, principal component analysis is used to improve kd-tree's performance. However, existing matching approaches fail to perform particularly for iris images. As iris is characterized by repeated occurrence of pattern, so there is a likelihood of two keypoints from different regions of iris being wrongly paired. This motivates the further research for improving matching performance of SIFT when applied to iris.

3.2 Iris Feature Extraction using SIFT

Due to expansion and contraction of pupil as a natural phenomenon, the texture pattern of iris undergo linear deformation. Thus, enhanced keypoint descriptor is required that performs for variation in scale along with other transformations. In this chapter, a local feature descriptor coined Scale Invariant Feature Transform (SIFT) [33] is used that provides stable set of features while being less sensitive to local image distortions. For robust feature extraction, the input iris image is localized for inner and outer boundary using image morphology [45]. The annular region between the iris circles is considered for feature extraction. The steps involved in feature extraction using SIFT are explained as follows:

3.2.1 Scale Space Extrema Detection

The keypoints are detected from annular iris image using cascade filtering approach. This is done to search stable features across all possible scales. To define the scale space, input iris image (I) is convolved with Gaussian kernel $G(x, y, \sigma)$ as defined by

$$L(x, y, \sigma) = G(x, y, \sigma) * I(x, y) \quad (3.1)$$

where $*$ is the convolution operation and σ defines the width of Gaussian filter. The Difference of Gaussian (DOG) images are computed from two nearby scales differentiated by constant multiplicative factor k

$$D(x, y, \sigma) = L(x, y, k\sigma) - L(x, y, \sigma) \quad (3.2)$$

The scale space generation for i and $i + 1$ octave is shown in Figure 3.1.

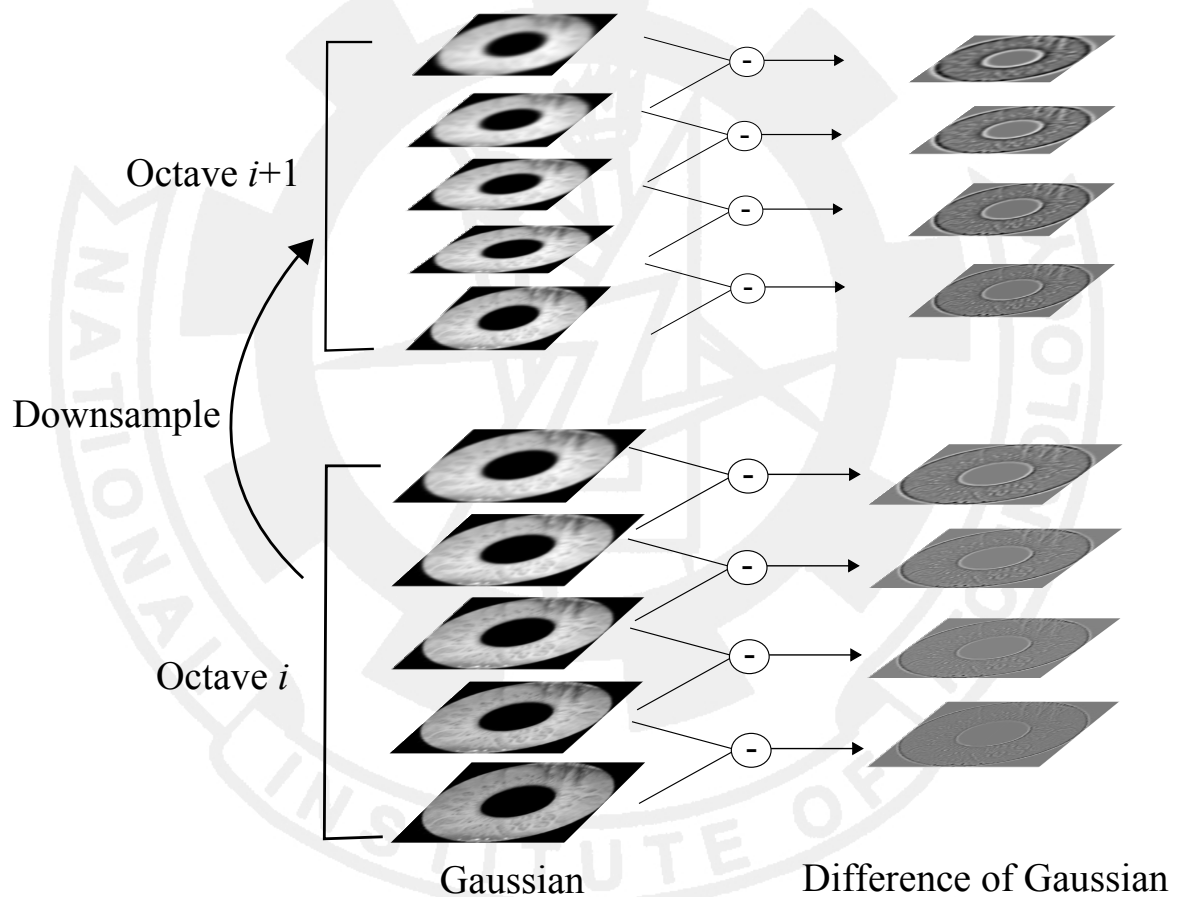


Figure 3.1: Scale space for i and $i+1$ octave using annular iris image

3.2.2 Keypoint Localization

DOG images are used to detect interest points with the help of local maxima and minima across different scales. Each pixel in DOG image is compared to 8 neighbors in the same scale and 9 neighbors in the scale above and below. The pixel is selected as a candidate keypoint if it is local maxima or minima in $3 \times 3 \times 3$ region.

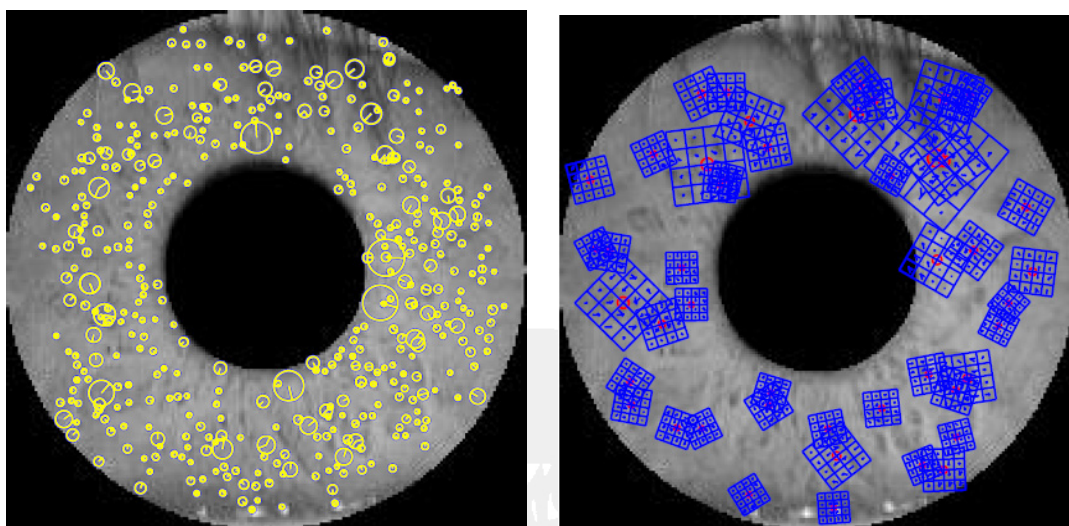


Figure 3.2: SIFT detected keypoints with change in scale (left) and oriented descriptor windows (right)

3.2.3 Orientation Assignment

Orientation is assigned to each keypoint location to achieve invariance to image rotations as descriptor can be represented relative to orientation. To determine keypoint orientation, a gradient orientation histogram is computed in the neighborhood of the keypoint. The scale of keypoint is used to select Gaussian smoothed image L . For each Gaussian smoothed image $L(x, y)$, magnitude ($m(x, y)$) and orientation ($\theta(x, y)$) are computed as

$$m(x, y) = \sqrt{(L(x+1, y) - L(x-1, y))^2 + (L(x, y+1) - L(x, y-1))^2} \quad (3.3)$$

$$\theta(x, y) = \tan^{-1} \left[\frac{L(x, y+1) - L(x, y-1)}{L(x+1, y) - L(x-1, y)} \right] \quad (3.4)$$

Orientation histogram is then formed for gradient orientation around each keypoint. The histogram has 36 bins for 360 degree range of orientations and each sample is weighted by gradient magnitude and Gaussian weighted circular window with σ of 1.5 times of scale of keypoint before adding it to histogram. Peaks in the histogram correspond to orientation and any other local peak within 80% of largest peak is used to create keypoint with the computed orientation. This is done to increase stability during matching [33]. The detected keypoints with change in scale and orientation is shown in Figure 3.2(left).

3.2.4 Keypoint Descriptor Computation

Once orientation has been selected, the feature descriptor is computed as a set of orientation histograms on 4×4 pixel neighborhoods. The orientation histograms are relative to the keypoint orientation as shown in Figure 3.2(right). These histograms contain 8 bins each and each descriptor contains an array of 16 histograms around the keypoint. This generates SIFT feature descriptor of $4 \times 4 \times 8 = 128$ elements. The descriptor vector is invariant to rotation, scaling and illumination.

3.3 Proposed Postmatching Pruning Approach

Iris contains many regions that are of similar texture. The major drawback of conventional SIFT matching is that it wrongly pairs keypoints from two different regions of iris just checking local features (as depicted in Figure 3.3). Thus, there is a stringent requirement to verify both spatial property (characterized by co-ordinates) and descriptor property (characterized by texture information) of a keypoint when it is being paired with another keypoint. This instigates the development of a new postmatching technique fusing the geometric and descriptor properties for pairing keypoints from the annular iris image. The pupil and iris circles are assumed to be concentric, hence all localized images have pixel size $2r \times 2r$, where r is the radius of iris. The pupil center as well as iris center are located at (r, r) . Therefore the localized images do not have transformation due to translation. However, there is a possibility of iris images being transformed due to rotation (tilt of subject's head), scaling (change in camera to eye distance) or both [39]. The SIFT matching algorithm matches keypoints that have similarity between the local descriptors (as discussed in Section 3.3.1) but fails to conform to spatial relationship. The removal (filtering) of impairments by the proposed approach retains only those pairs that are more probable to be potential.

3.3.1 Nearest Neighbor SIFT Keypoint Pairing

The matching algorithm plays a significant role in any biometric system. In local feature matching, the total number of paired keypoints is used to find the authenticity of an

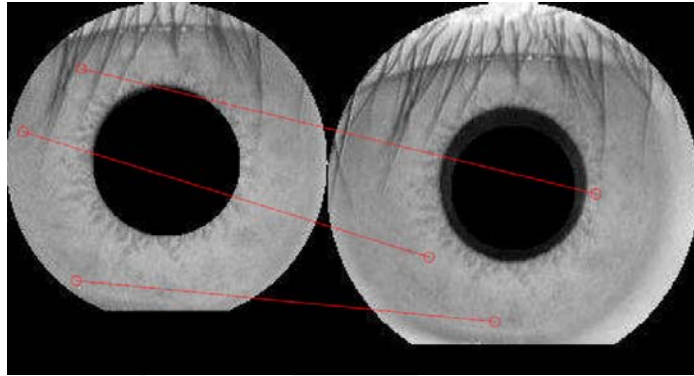


Figure 3.3: Sample impairments generated by SIFT matching

individual. Let I be the set of all images available in the iris database. For understanding, I_m be a gallery iris image and I_n be a probe iris image where $I_m, I_n \in I$. Let K_m be the set of p keypoints found in I_m and K_n be the set of q keypoints found in I_n by applying SIFT detector. Let D_m and D_n denote the set containing keypoint descriptors for each keypoint in K_m and K_n respectively. In SIFT matching, for each element in D_m the Euclidean distance is found with every element in D_n . The nearest neighbor approach pairs the i^{th} element in D_m with j^{th} element in D_n , iff the descriptor distance between the two (after multiplying with a threshold) is minimum [33]. The details of the algorithm is explained in Algorithm 3.1. Let R be the ordered set containing the matches between D_m and D_n by SIFT matching. Let η be the number of matches found where $\eta \in [0, \min(p, q)]$. This approach performs moderately well for unconstrained iris recognition [39]. However, as SIFT determines image similarity using only local features, it may wrongly pair (impair) some keypoints for iris. Thus, existing approach is modified which removes impaired matches for better recognition accuracy.

3.3.2 Proposed Filtering of Keypoints

Information of the spatial locations of keypoints is used for pruning wrong pairs from SIFT. The proposed pruning algorithm takes the keypoint pairs from SIFT as input, and removes the impairments, therefore leaving behind a potential subset of SIFT pairs as output. The proposed approach performs filtering in two different ways. In the first method, the impairments of SIFT pairs are detected using angular filtering criteria. In the second method, the impairments of SIFT pair are detected by scale filtering approach. These two

Algorithm 3.1 SIFT_Matching**Input:** D_m : Keypoint descriptors for I_m , D_n : Keypoint descriptors for I_n **Output:** R : Keypoint pairs from SIFT

```

1:  $\omega \leftarrow$  Threshold for pairing
2: while  $i \leq |D_m|$  and  $|D_n| \neq 0$  do
3:   for  $j := 1$  to  $|D_n|$  do
4:      $E_j \leftarrow \sqrt{(D_{m_i} - D_{n_j})^2}$ 
5:   end for
6:    $[min\_value\ index] \leftarrow$  minimum( $E$ )
7:    $E_{index} \leftarrow min\_value \times \omega$ 
8:    $[min\_value\ new\_index] \leftarrow$  minimum( $E$ )
9:   if  $index = new\_index$  then
10:     $R_i \leftarrow (i, index)$ 
11:     $D_m \leftarrow D_m - D_{m_i}$ 
12:     $D_n \leftarrow D_n - D_{n_{index}}$ 
13:   end if
14: end while
15: return  $R$ 

```

approaches are also tested to be applied in sequence to remove impairments from SIFT pairs. As seen experimentally, the combination of angular and scale filtering generates better result than the filtering processes applied singularly.

Proposed Angular Filtering

In this stage gradient based filtering is performed to remove impairments from R (set containing SIFT pairs). This is done to include spatial property of keypoints for finding the accurate matches. To compute gradient for each pair of keypoints (i, j) in R , the angles are obtained from respective image centers (r, r) . Thus, θ_i is computed from I_m and ϕ_j is computed from I_n . The angle of rotation for k^{th} pair is calculated as $\gamma_k = (\phi_j - \theta_i) \bmod 360^\circ$ (depicted in Figure 3.4(a)). Considering SIFT to be completely *flawless* (due to robustness property, no false match is found) and *efficient* (due to property of repeatability, all possible matches are found) [33]; the value of γ_k derived should be same $\forall k$. But in practice, SIFT does not give such precise matches. Thus, it is difficult to obtain unique value of γ even when I_m and I_n belong to the same subject. Rather a distribution of γ is obtained.

A histogram is plotted with horizontal axis comprising bins with a range of values of γ , and vertical axis comprising number of matches falling in a particular bin as shown in

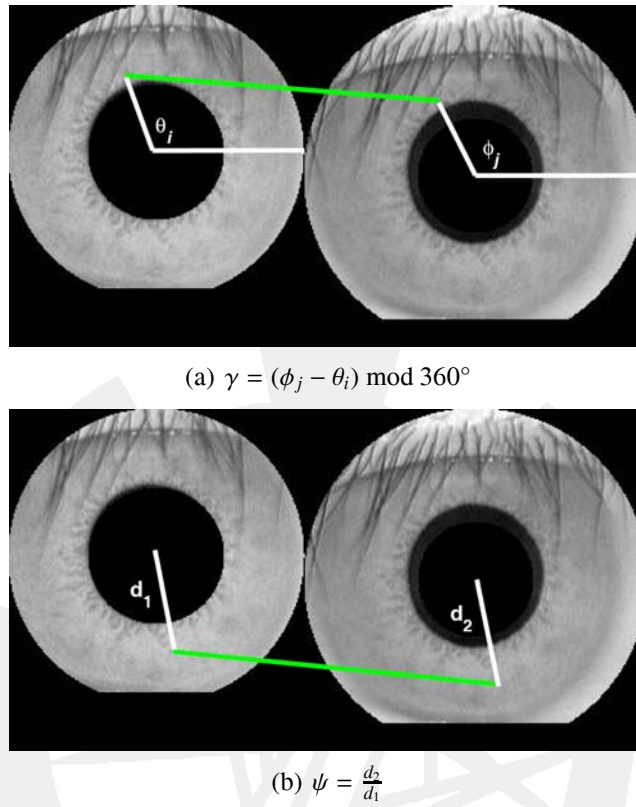


Figure 3.4: (a) Gradient(γ) computation in Section 3.3.2, (b) Local scaling factor(ψ) computation in Section 3.3.2

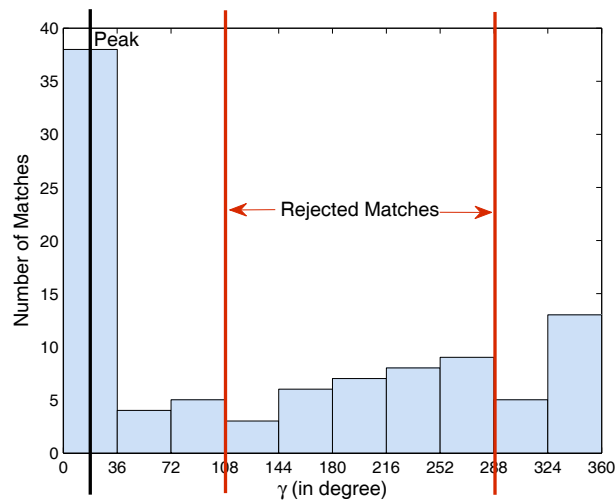


Figure 3.5: Distribution of γ for number of matches between two instances of the same subject (taken from CASIAV3)

Figure 3.5. The number of bins in the histogram (N_{bins}) is subject to implementation issue. In the proposed system, N_{bins} is taken as 10. The distribution of γ gives a single peak in

case the two iris images (I_m and I_n) are from the same subject. In contrast, no distinct peak should be found in case the two iris images are from different subjects.

In the above mentioned histogram peak detection process, there may be problem due to discretization of bins. To avoid that, two adjacent bins of the peak are combined to improve peak density (number of matches). The idea is to find whether the density of the peak exceeds the boundary criteria. It is inferred that a peak is strong if the density exceeds certain higher bound ($hp\%$ of total number of matches). Likewise peak is weak if the density is less than a lower bound ($lp\%$ of total number of matches). If a strong peak is found, an angular range is specified around the peak. Those matches in R for which γ are not within the angular range are declared to be impaired and pruned from R to generate $R_{angular}$. For example, as observed in histogram in Figure 3.5, the peak is found at 0^{th} bin which represents gradient value of 0° to 36° with a central value of 18° . Hence only those pairs having angular range between $(18 \pm 90) \bmod 360^\circ$ are retained as accurate matches. Rest of the pairs in R are pruned. Thus, it is evident that $R_{angular} \subseteq R$ after removing some impairments (as proposed in Algorithm 3.2). Figure 3.6(b) shows paired keypoints in $R_{angular}$ with considerable reduction of η from Figure 3.6(a). If no strong peak is found in the histogram of γ , then all matches in R are inferred to be removed. As a result $R_{angular}$ becomes empty in that case.

Proposed Scale Filtering

In this stage further filtering of set of SIFT pairs (R) is performed on the basis of global and local scaling factor between the gallery and probe images. The global scaling factor (sf) between two images is defined as ratio of probe iris radius (r_n) to gallery iris radius (r_m). A scale range with certain tolerance around sf is empirically taken to handle aliasing artifact. From implementation perspective, the scale range is taken as $(sf \pm 0.2)$.

During filtering, for each element in R , two Euclidean distances are calculated as, (a) d_1 : distance of i^{th} keypoint of I_m from its center and (b) d_2 : distance of j^{th} keypoint of I_n from its center. Local scaling factor (ψ) for each element of R is calculated as $\psi = d_2/d_1$ (as shown in Figure 3.4(b)). Matches having ψ within scale range $(sf \pm 0.2)$ qualifies to be potential and stored in R_{scale} , else are labeled as faulty and pruned as described in

Algorithm 3.2 Angular_Filtering

Input: R : Keypoint pairs from SIFT

Output: $R_{angular}$: Keypoints paired after angular filtering

```

1:  $N_{bins} \leftarrow$  Number of bins
2:  $hp \leftarrow$  High percentage threshold
3:  $lp \leftarrow$  Low percentage threshold
4:  $G_{range} \leftarrow$  Gradient acceptance range
5: for  $k := 1$  to  $|R|$  do
6:    $\theta_i = \text{Gradient}(i, I_m)$   $\{i^{th}$  keypoint of iris  $I_m\}$ 
7:    $\theta_j = \text{Gradient}(j, I_n)$   $\{j^{th}$  keypoint of iris  $I_n\}$  {Algorithm 3.3}
8:    $\gamma_k \leftarrow (\theta_j - \theta_i)$ 
9:    $bin \leftarrow \lfloor \frac{\gamma_k}{(360/N_{bins})} \rfloor$ 
10:   $hist[bin] \leftarrow hist[bin] + 1$  {Histogram creation}
11: end for
12:  $[count_{max} \ bin_{max}] \leftarrow \max(hist)$ 
13:  $peak_{merge} \leftarrow hist[bin_{max}] + hist[(bin_{max} \pm 1) \bmod N_{bins}]$ 
14: if  $(peak_{merge} > |R| \times hp)$  then
15:    $F \leftarrow \{R : \gamma \notin (bin_{max} \pm G_{range}) \bmod 360\}$ 
16:    $R_{inter} \leftarrow R - F$ 
17: else
18:   if  $(peak_{merge} < |R| \times lp)$  then
19:      $R_{angular} \equiv \phi$ 
20:   end if
21: end if
22: return  $R_{angular}$ 
    
```

Algorithm 3.3 Find_Gradient

Input: k : keypoint index, I : iris image

Output: θ : Gradient of k^{th} keypoint

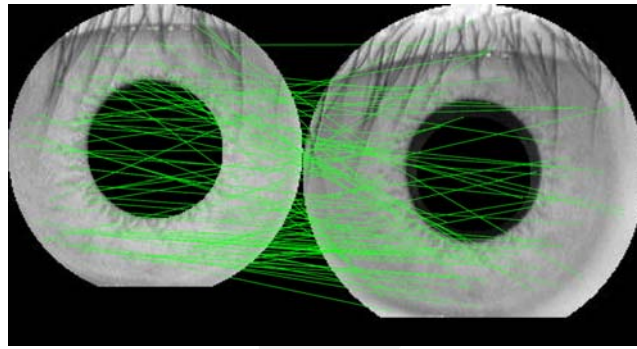
```

1:  $[x_c \ y_c] \leftarrow$  center of  $I$ 
2:  $[x_k \ y_k] \leftarrow$  coordinates of  $k$ 
3:  $y_d \leftarrow (y_k - y_c)$ 
4:  $x_d \leftarrow (x_k - x_c)$ 
5:  $\theta \leftarrow \tan^{-1} \left( \frac{y_d}{x_d} \right)$ 
6: return  $\theta$ 
    
```

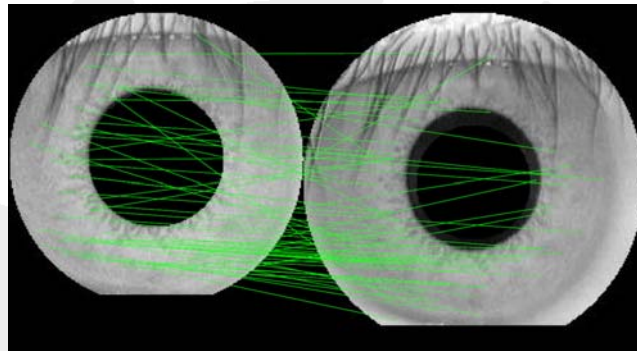
Algorithm 3.4. Figure 3.6(c) shows paired keypoints in R_{scale} after reduction of η from Figure 3.6(a).

Combining Angular and Scale Filtering

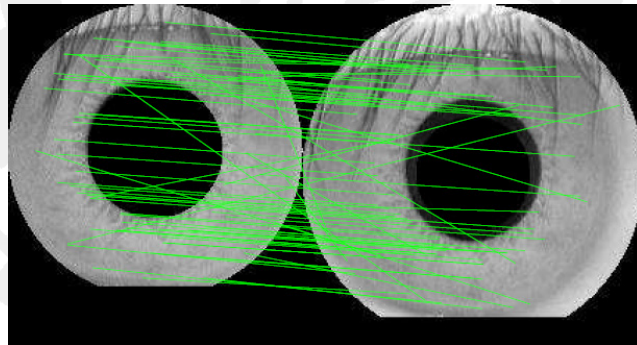
The above mentioned pruning schemes can be applied in sequence. Angular filtering approach is first applied to set of SIFT pairs R . Let the resulting set of pairs after pruning



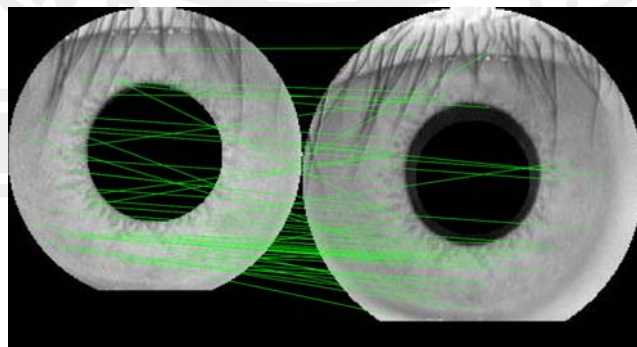
(a) Applying SIFT matching: $\eta = 98$



(b) Applying Angular filtering: $\eta = 65$



(c) Applying Scale filtering: $\eta = 78$



(d) Applying Angular and Scale filtering: $\eta = 54$

Figure 3.6: Matches (η) obtained by proposed pruning schemes (for two instances of same individual taken from CASIAV3)

Algorithm 3.4 Scale_Filtering**Input:** R : Keypoint pairs from SIFT**Output:** R_{scale} : Keypoints paired after scale filtering

```

1:  $r_m \leftarrow$  iris radius of  $I_m$ 
2:  $r_n \leftarrow$  iris radius of  $I_n$ 
3:  $S_{range} \leftarrow$  Scale acceptance range
4:  $sf = \frac{r_n}{r_m}$ 
5: for  $k := 1$  to  $|R_{inter}|$  do
6:    $d_i = \text{Distance}(i, I_m)$   $\{i^{th}$  keypoint of iris  $I_m\}$ 
7:    $d_j = \text{Distance}(j, I_n)$   $\{j^{th}$  keypoint of iris  $I_n\}$  {Algorithm 3.5}
8:    $\psi_k \leftarrow d_j/d_i$ 
9: end for
10:  $F \leftarrow \{R : \psi \notin (sf \times (1 \pm S_{range}))\}$ 
11:  $R_{scale} \leftarrow R - F$ 
12: return  $R_{scale}$ 

```

Algorithm 3.5 Find_Distance**Input:** k : keypoint index, I : iris image**Output:** d : Distance of k^{th} keypoint from iris center

```

1:  $[x_c \ y_c] \leftarrow$  center of  $I$ 
2:  $[x_k \ y_k] \leftarrow$  coordinates of  $k$ 
3:  $d \leftarrow \sqrt{(x_k - x_c)^2 + (y_k - y_c)^2}$ 
4: return  $d$ 

```

be R_{inter} . This set is fetched as input to the scale filtering approach. Scale filtering approach would further prune some pairs from R_{inter} and finally would generate R_{final} , say. It is evident that $R_{final} \subseteq R_{inter} \subseteq R$. Figure 3.6(d) shows paired keypoints in R_{scale} after reduction of η from Figure 3.6(a). The obtained output R_{final} is experimentally claimed to give a better imposter-genuine score separation than conventional SIFT pair R gives.

3.4 Experimental Results

The experiments regarding SIFT keypoint matching are tested on 100 localised images of CASIAV3 database that generates $\binom{100}{2} = 4,950$ test cases. Same experiments are repeated for 80 localised images from BATH database that generates $\binom{80}{2} = 3,160$ test cases. The experiments are carried out in four sequential phases. In the first phase the performance of iris matching is tested when matching is done using conventional SIFT approach. The results obtained are described in Section 3.4.1. In the next phase of experiment, the

SIFT matching is followed by filtering of pairs on the knowledge of angular information of keypoints as described in Section 3.3.2. The results achieved in this phase of the experiment is traced in Section 3.4.2. Results shown in the Section 3.4.3 explains the outcome of the third phase of the experiment, where the accuracy of matching is measured by applying SIFT matching followed by scale filtering of pairs (as previously explained in Section 3.3.2). Finally in the last phase of the experiment, the recognition accuracy is measured by applying SIFT followed by applying both angular and scale filtering of pairs. The results of this phase are discussed in Section 3.4.4.

3.4.1 Experiment I: Applying conventional SIFT

The gallery and probe iris images are matched using conventional SIFT matching approach following the notion of matching nearest neighbors. Here the images that have high texture similarity are likely to be wrongly paired thus increasing error rates of the system. The iris recognition system performs with an accuracy of 85.81% on CASIAV3 database. The d' measure of 1.20 is obtained for CASIAV3 database. Likewise, for BATH database an accuracy of 97.04% with FAR of 1.57% is obtained. As Table 3.4.4 depicts, SIFT works well for cooperative iris images of BATH database (with 97.1% rank-1 accuracy); but the performance degrades for occluded iris images of CASIAV3 database (with 67.5% rank-1 accuracy only).

3.4.2 Experiment II: Applying Angular filtering

To improve the performance of the system, the objective of the proposed research is to reduce false acceptances. In second level of experiments, the impairments are removed using angular filtering which significantly reduces FAR to 2.92% and 0.92% for CASIAV3 and BATH respectively. The d' measure improves to 2.44 for CASIAV3 database. This improves accuracy but leaves behind the scope for further improvement of FAR.

3.4.3 Experiment III: Applying Scale filtering

Due to scale filtering, FAR reduces reasonably to 5.45% and 0.59% for CASIAV3 and BATH respectively. The accuracy improvement is significant with slight increase in matching time. The accuracy values are plotted against change in number of matches as shown in Figure 3.7(a) and Figure 3.8(a) for CASIAV3 and BATH databases respectively. The confidence of rank-1 recognition is 91.00% and 97.10% for CASIAV3 and BATH databases respectively.

3.4.4 Experiment IV: Applying combined Angular and Scale filtering

The above two types of filtering are applied together for removing the impairments falling to either of the category. The Receiver Operating Characteristic (ROC) curves [46] for these four different stages for CASIAV3 and BATH are shown in Figure 3.7(b) and Figure 3.8(b) respectively. The distribution of genuine and imposter scores for SIFT, angular filtering, scale filtering and the result of combined angular and scale filtering on CASIAV3 database are shown in Figure 3.9(a), Figure 3.9(b), Figure 3.9(c) and Figure 3.9(d) respectively. Similar results are observed for BATH database as shown in Figure 3.10(a), Figure 3.10(b), Figure 3.10(c) and Figure 3.10(d). The proposed scheme makes the system rank-3 bounded even for occluded iris images of CASIAV3 database as it can be observed from Table 3.4.4, which marks high improvement with respect to conventional SIFT.

Table 3.1: Performance comparison of SIFT matching and proposed post matching

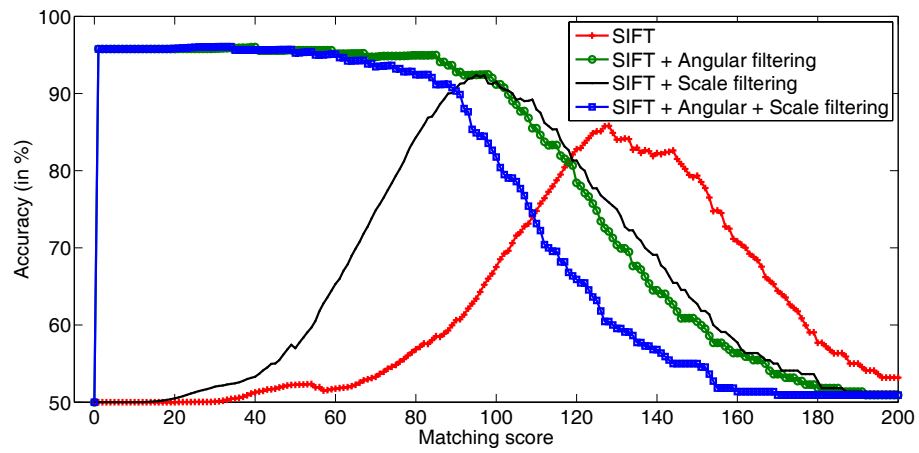
Databases →	CASIAV3				BATH			
Approach ↓	FAR	FRR	ACC	d'	FAR	FRR	ACC	d'
SIFT	17.48	10.91	85.81	1.20	1.57	4.35	97.04	2.73
Angular filtering	02.49	05.45	96.03	2.46	0.97	6.09	96.47	2.81
Scale filtering	06.10	09.10	92.41	1.44	1.01	4.35	97.32	2.88
Angular + Scale filtering	02.39	05.45	96.08	2.20	1.34	4.35	97.15	2.90

Table 3.2: Rank- k identification rate for SIFT matching approach and proposed postmatch pruning approaches

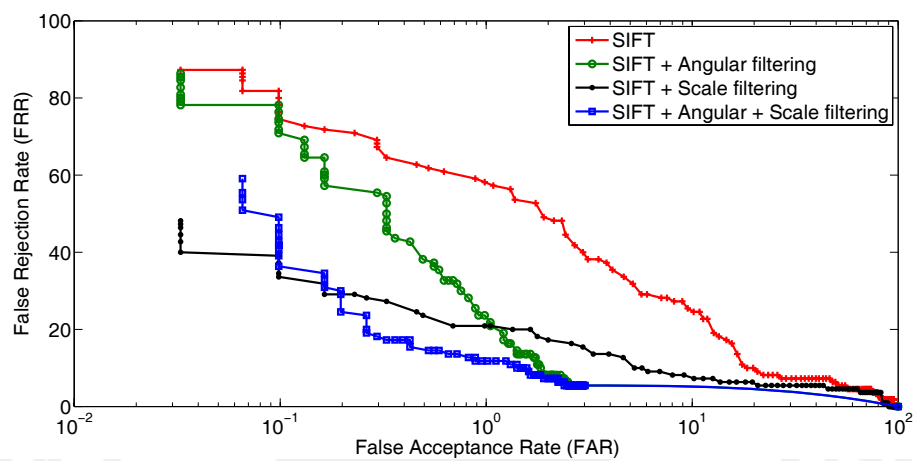
Rank ↓	CASIAV3				BATH			
	SIFT	Angular	Scale	Angular + Scale	SIFT	Angular	Scale	Angular + Scale
1	0.675	0.833	0.910	0.912	0.912	1.000	0.971	0.971
2	0.737	0.923	0.961	0.941	0.941	1.000	0.971	1.000
3	0.800	0.948	0.961	1.000	1.000	1.000	1.000	1.000
4	0.812	0.948	0.987	1.000	1.000	1.000	1.000	1.000
5	0.837	0.948	1.000	1.000	1.000	1.000	1.000	1.000
10	0.887	0.948	1.000	1.000	1.000	1.000	1.000	1.000
20	0.912	1.000	1.000	1.000	1.000	1.000	1.000	1.000
50	0.950	1.000	1.000	1.000	1.000	1.000	1.000	1.000
77	1.000	1.000	1.000	1.000	1.000	1.000	1.000	1.000

3.5 Summary

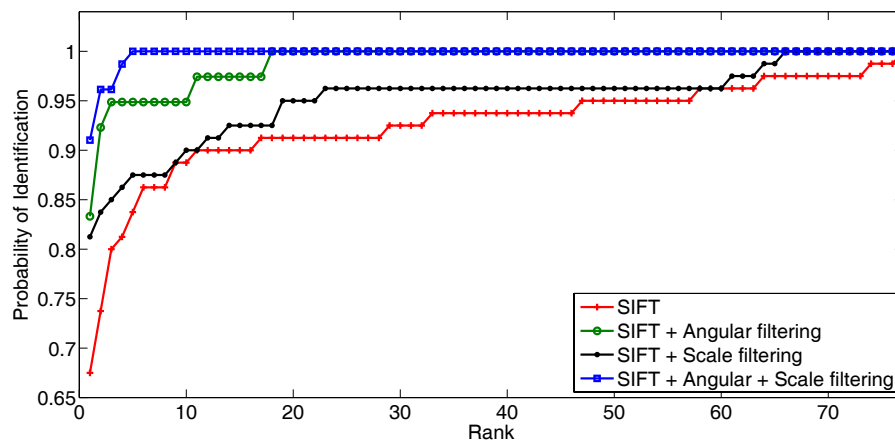
In this chapter, a novel postmatch impairment pruning technique is proposed that improvises performance of conventional SIFT for iris recognition by removing wrong pairs. The above explained four step experimental results justify the claim of the chapter that the proposed postfiltering of SIFT pairs effectively filters out impairments on the basis of their spatial information. As a result the pairs left after filtering are more potential to separate between genuine and imposter matching scores. Lastly, the approach in this chapter partially prunes faulty matches, there can be some other technique devised in future to remove those faulty matches that are not being pruned by this approach. So it can be said that the proposed algorithm is completely flawless, i.e., matches which are removed are guaranteed to be wrong matches; whereas the algorithm is not completely efficient, i.e., all impairments by SIFT are not guaranteed to be filtered. However, the gain in accuracy is substantial which marks applicability of pruning of SIFT impairments for unconstrained iris recognition.



(a) Accuracy curve

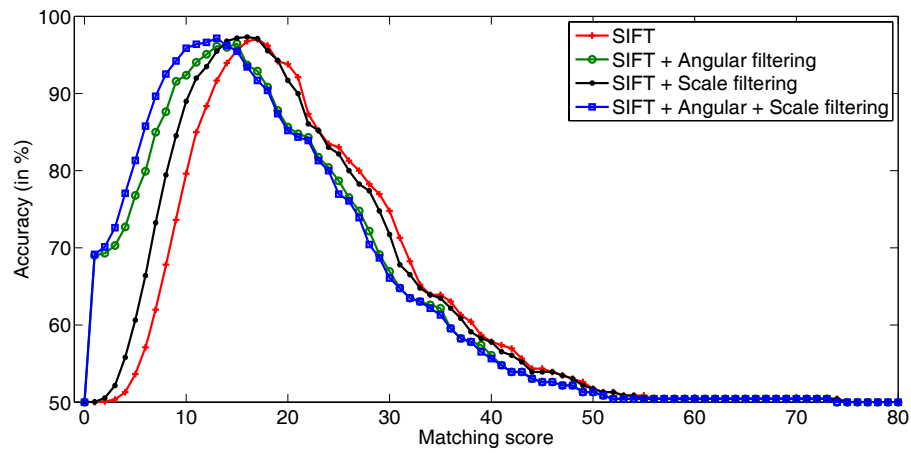


(b) ROC curve

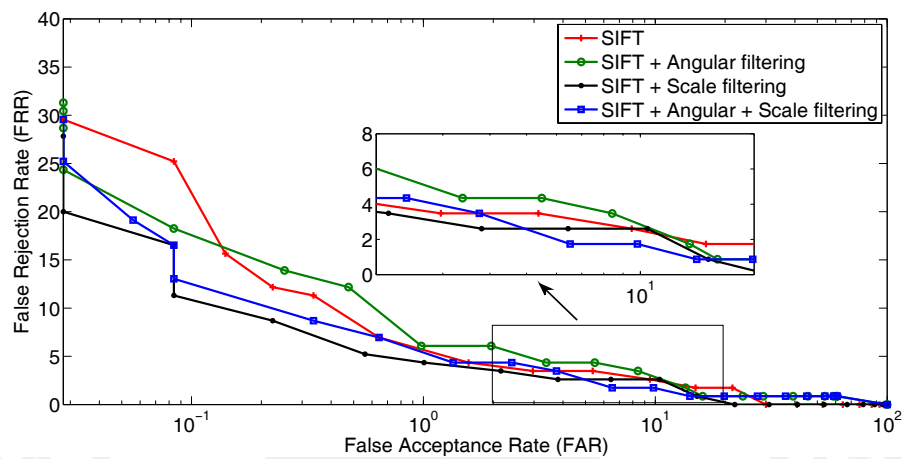


(c) CMC curve

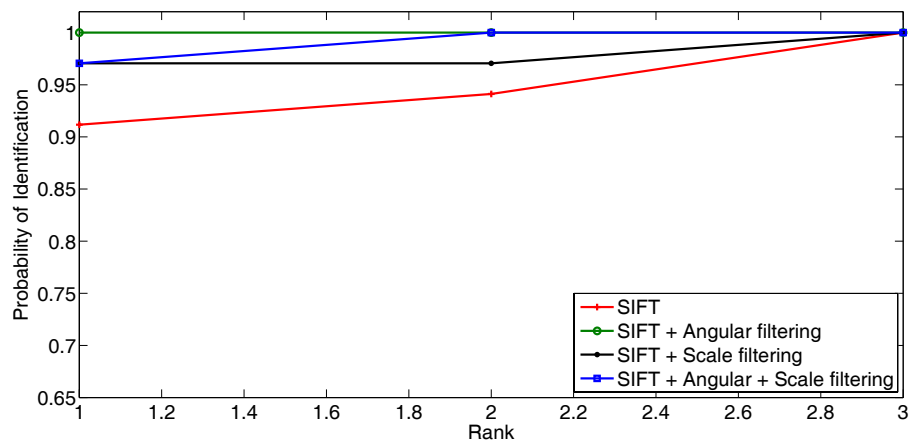
Figure 3.7: Graphical plots for CASIAV3 database at different stages



(a) Accuracy curve

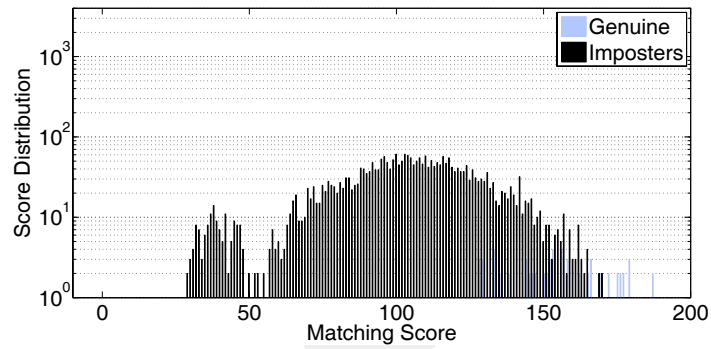


(b) ROC curve

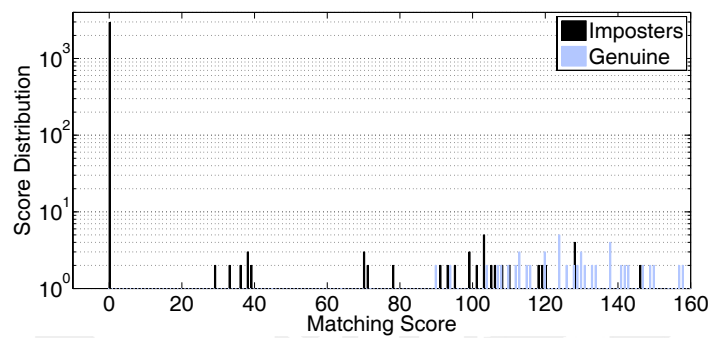


(c) CMC curve

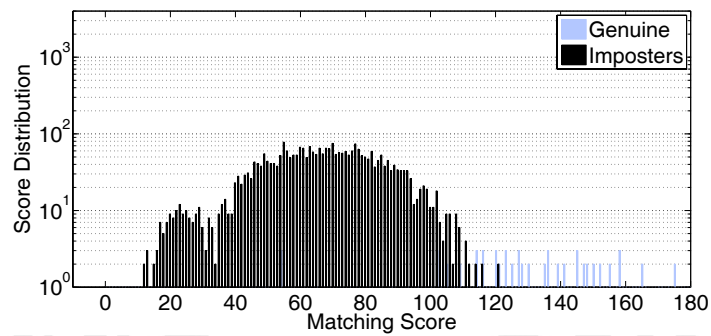
Figure 3.8: Graphical plots for BATH database at different stages



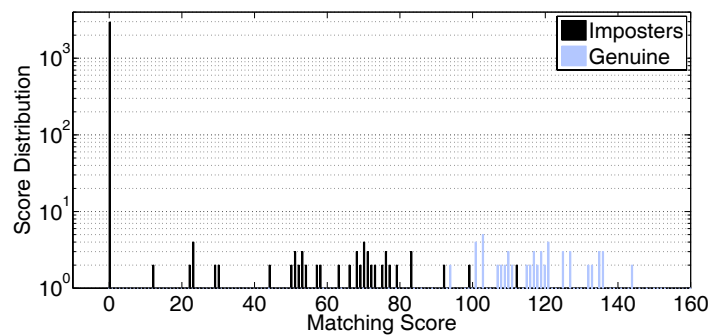
(a) SIFT



(b) Angular filtering

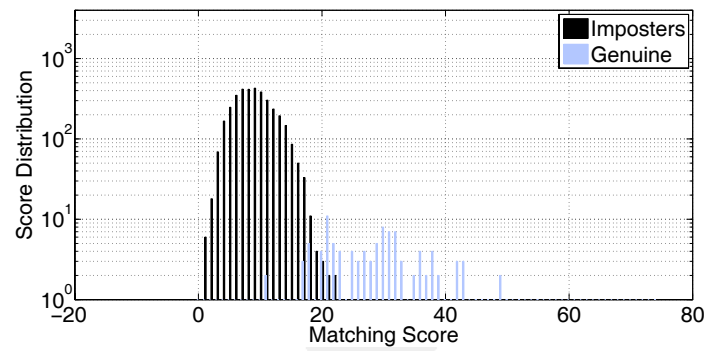


(c) Scale filtering

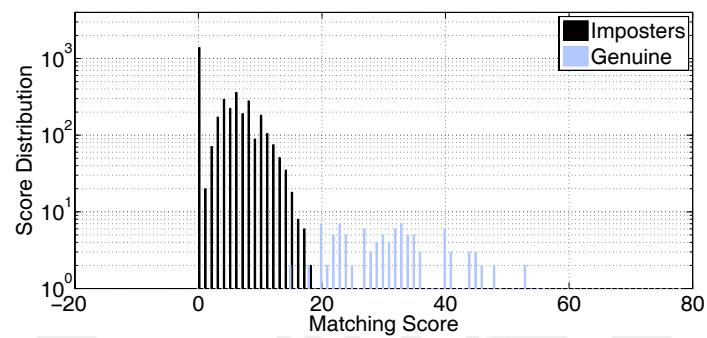


(d) Angular + Scale filtering

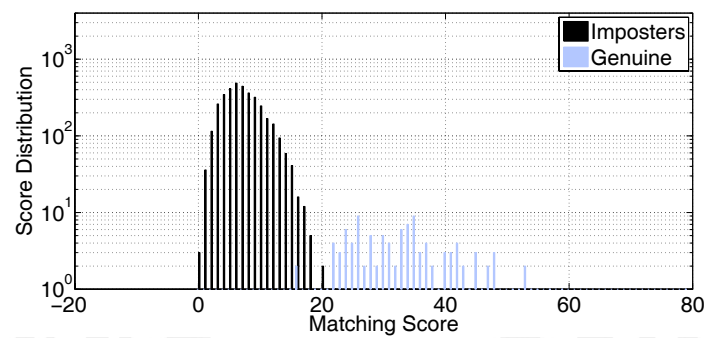
Figure 3.9: Distribution for genuine and imposter scores for CASIAV3 database



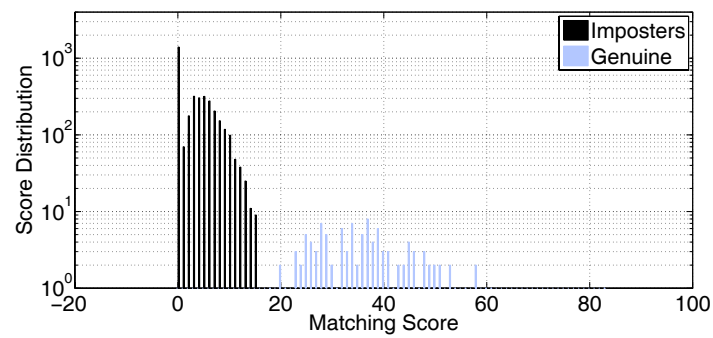
(a) SIFT



(b) Angular filtering



(c) Scale filtering



(d) Angular + Scale filtering

Figure 3.10: Distribution for genuine and imposter scores for BATH database

Chapter 4

Conclusions and Future Work

The thesis approaches towards developing robust localization scheme for unconstrained iris recognition. The proposed localization approach is experimented against two publically available databases. It is working fast for non-cooperative images of CASIAV3 database. The proposed approach efficiently detects annular region containing iris. But the proposed approach does not take into consideration the detection and removal of eyelid and eyelashes. The approach describes lower and upper iris boundaries by two concentric circles. However in case of non-centred gaze of the subject, the shape of iris is better described by an ellipse. Also the pupil centre and iris centre are non-overlapping in such cases. The proposed approach can further be extended by fitting ellipses rather than circles to describe iris boundaries and by removing the eyelids to obtain a more precise region of interest.

The second proposed approach in this thesis deals with pruning SIFT impairments. The pairs removed by the algorithm are guaranteed to be wrong pairs. However all wrong pairs by SIFT are not pruned by the algorithm due to certain impairment tolerance factors implicitly used in the algorithm. Some tolerable wrong matches may exist even after running the algorithm. The proposed algorithm increases the separability between imposter and genuine scores by SIFT with the trade-off of extra computation time of wrong matches. Another remarkable fact is that the proposed pruning approach can also work with other local feature techniques like SURF.

The proposed localization approach and impairment pruning approach are thoroughly tested on iris images available from BATH and CASIAV3 databases. The approaches have

yet not been tested against small and poor quality images of UBIRIS version 1.

To conclude with this thesis, the proposed approaches have been critically analysed and few limitations have been observed as discussed above. Exploring and refining these limitations further research in the proposed area.



Bibliography

- [1] A. K. Jain, P. Flynn, and A. A. Ross. *Handbook of Biometrics*. Springer-Verlag New York, Inc., Secaucus, NJ, USA, 2007.
- [2] Chinese Academy of Sciences' Institute of Automation (CASIA) Database. <http://www.cbsr.ia.ac.cn/english/IrisDatabase.asp>.
- [3] L. Flom and A. Safir. Iris recognition system. U.S. Patent 4,641,349, 1987.
- [4] G. Xu, Z.F. Zhang, and Y.D. Ma. Automatic iris segmentation based on local areas. In *International Conference on Pattern Recognition*, volume 4, pages 505–508. IEEE Computer Society, 2006.
- [5] Kevin W. Bowyer, Karen Hollingsworth, and Patrick J. Flynn. Image understanding for iris biometrics: A survey. *Computer Vision and Image Understanding*, 110(2):281 – 307, 2008.
- [6] M. Golfarelli, D. Maio, and D. Maltoni. On the error-reject trade-off in biometric verification systems. *IEEE Transactions on Pattern Analysis and Machine Intelligence*, 19(7):786–796, 1997.
- [7] A. Y. Johnson, J. Sun, and A. F. Bobick. Predicting Large Population Data Cumulative Match Characteristic Performance from Small Population Data. In *AVBPA*, pages 821–829, 2003.
- [8] H. Proenca and L. A. Alexandre. UBIRIS: A noisy iris image database. In *13th International Conference on Image Analysis and Processing - ICIAP 2005*, volume LNCS 3617, pages 970–977. Springer, 2005.
- [9] BATH University Database. <http://www.bath.ac.uk/elec-eng/research/sipg/irisweb>.
- [10] Indian Institute of Technology Kanpur Database. <http://www.cse.iitk.ac.in/users/biometrics>.
- [11] L. Ma, T. Tan, Y. Wang, D. Zhang, and C. Boyce. Critique: Efficient iris recognition by characterizing key local variations. *IEEE Transactions on Image Processing*, 13(6), 2008.
- [12] R.P. Wildes. Iris recognition: an emerging biometric technology. *Proceedings of the IEEE*, 85(9):1348–1363, 1997.
- [13] H. Proenca and L.A. Alexandre. Iris recognition: An analysis of the aliasing problem in the iris normalization stage. In *International Conference on Computational Intelligence and Security*, volume 2, pages 1771–1774, 2006.
- [14] J. Daugman. The importance of being random: statistical principles of iris recognition. *Pattern Recognition*, 36(2):279 – 291, 2003.

- [15] Y. Huang, S. Luo, and E. Chen. An efficient iris recognition system. In *International Conference on Machine Learning and Cybernetics*, volume 1, pages 450–454, 2002.
- [16] Y. Liu, S. Yuan, X. Zhu, and Q. Cui. A practical iris acquisition system and a fast edges locating algorithm in iris recognition. In *20th IEEE Conference on Instrumentation and Measurement Technology*, volume 1, pages 166–168, 2003.
- [17] H. Sung, J. Lim, J. Park, and Y. Lee. Iris recognition using collarete boundary localization. In *17th International Conference on Pattern Recognition*, volume 4, pages 857–860, 2004.
- [18] X. Liu, K.W. Bowyer, and P.J. Flynn. Experiments with an improved iris segmentation algorithm. In *Fourth IEEE Workshop on Automatic Identification Advanced Technologies*, pages 118–123, 2005.
- [19] X. Feng, C. Fang, X. Ding, and Y. Wu. Iris localization with dual coarse-to-fine strategy. In *18th International Conference on Pattern Recognition*, volume 4, pages 553–556, 2006.
- [20] T.A. Camus and R. Wildes. Reliable and fast eye finding in close-up images. In *16th International Conference on Pattern Recognition*, volume 1, pages 389–394, 2002.
- [21] B. Bonney, R. Ives, D. Etter, and D. Yingzi. Iris pattern extraction using bit planes and standard deviations. In *Conference Record of the Thirty-Eighth Asilomar Conference on Signals, Systems and Computers*, volume 1, 2004.
- [22] H. Proenca and L.A. Alexandre. Iris segmentation methodology for non-cooperative recognition. *IEE Proceedings on Vision, Image and Signal Processing*, 153(2):199–205, 2006.
- [23] S.J. Pundlik, D.L. Woodard, and S.T. Birchfield. Non-ideal iris segmentation using graph cuts. In *IEEE Computer Society Conference on Computer Vision and Pattern Recognition Workshops*, pages 1–6, 2008.
- [24] Zhaofeng He, Tieniu Tan, Zhenan Sun, and Xianchao Qiu. Toward accurate and fast iris segmentation for iris biometrics. *Pattern Analysis and Machine Intelligence, IEEE Transactions on*, 31(9):1670–1684, sept. 2009.
- [25] Liu Jin, Fu Xiao, and Wang Haopeng. Iris image segmentation based on k-means cluster. In *Intelligent Computing and Intelligent Systems (ICIS), 2010 IEEE International Conference on*, volume 3, pages 194–198, oct. 2010.
- [26] Fei Tan, Zhengming Li, and Xiaoqin Zhu. Iris localization algorithm based on gray distribution features. In *Progress in Informatics and Computing (PIC), 2010 IEEE International Conference on*, volume 2, pages 719–722, dec. 2010.
- [27] Q. Tian, Q. Pan, Y. Cheng, and Q. Gao. Fast algorithm and application of hough transform in iris segmentation. In *International Conference on Machine Learning and Cybernetics*, volume 7, pages 3977–3980, 2004.
- [28] M. Tuceryan. Moment-based texture segmentation. *Pattern Recognition Letters*, 15(7):659–668, 1994.
- [29] R.C. Gonzalez and R.E. Woods. *Digital Image Processing (3rd Edition)*. Prentice Hall, 2008.

- [30] B. Lipinski. Iris recognition: Detecting the pupil. Connexions website, 2004. <http://cnx.org/content/m12487/1.4/>.
- [31] L. Ma, T. Tan, Y. Wang, and D. Zhang. Efficient iris recognition by characterizing key local variations. *IEEE Transactions on Image Processing*, 13(6):739–750, 2004.
- [32] H. Proenca and Luis A. Alexandre. Toward noncooperative iris recognition: A classification approach using multiple signatures. *IEEE Transactions on Pattern Analysis and Machine Intelligence*, 29:607–612, 2007.
- [33] D.G. Lowe. Distinctive image features from scale-invariant keypoints. *International Journal of Computer Vision*, 60(2):91, November 2004.
- [34] J. Daugman. New methods in iris recognition. *IEEE Transactions on Systems, Man, and Cybernetics, Part B: Cybernetics*, 37(5):1167–1175, 2007.
- [35] Z.A. Sun, T.N. Tan, and Y.H. Wang. Robust encoding of local ordinal measures: A general framework of iris recognition. In *ECCV Workshop on Biometric Authentication*, pages 270–282, 2004.
- [36] P. Yao, J. Li, X. Ye, Z. Zhuang, and B. Li. Iris recognition algorithm using modified log-gabor filters. In *Proceedings of the 18th International Conference on Pattern Recognition*, pages 461–464, 2006.
- [37] D.M. Monro, S. Rakshit, and D. Zhang. DCT-based iris recognition. *IEEE Transactions on Pattern Analysis and Machine Intelligence*, 29(4):586–595, 2007.
- [38] C. Loic, L. Torres, and M. Robert. Person identification technique using human iris recognition. In *Vision Interface*, pages 294–299, 2002.
- [39] C. Belcher and Y. Du. Region-based SIFT approach to iris recognition. *Optics and Lasers in Engineering*, 47(1):139–147, 2009.
- [40] Hunny Mehrotra, G. S. Badrinath, Banshidhar Majhi, and Phalguni Gupta. An efficient iris recognition using local feature descriptor. In *Proceedings of the 16th IEEE international conference on Image processing, ICIP'09*, pages 1937–1940, 2009.
- [41] Herbert Bay, Andreas Ess, Tinne Tuytelaars, and Luc Van Gool. Speeded-up robust features (surf). *Computer Vision and Image Understanding*, 110(3):346–359, 2008. Similarity Matching in Computer Vision and Multimedia.
- [42] Minjie Li, Liqiang Wang, and Ying Hao. Image matching based on sift features and kd-tree. In *Computer Engineering and Technology (ICCET), 2010 2nd International Conference on*, volume 4, pages V4–218–V4–222, april 2010.
- [43] Marius Muja and David G. Lowe. Fast approximate nearest neighbors with automatic algorithm configuration. In *In VISAPP International Conference on Computer Vision Theory and Applications*, pages 331–340, 2009.
- [44] C. Silpa-Anan and R. Hartley. Optimised kd-trees for fast image descriptor matching. In *Computer Vision and Pattern Recognition, 2008. CVPR 2008. IEEE Conference on*, pages 1–8, june 2008.

- [45] Sambit Bakshi, Hunny Mehrotra, and Banshidhar Majhi. Real-time iris segmentation based on image morphology. In *Proceedings of the 2011 International Conference on Communication, Computing & Security*, ICCCS '11, pages 335–338. ACM, 2011.
- [46] A.K. Jain, P. Flynn, and A.A. Ross. *Handbook of Biometrics*. Springer-Verlag New York, Inc., Secaucus, NJ, USA, 2007.



Dissemination

Published

1. **Sambit Bakshi**, Hunny Mehrotra, and Banshidhar Majhi. Real-time iris segmentation based on image morphology. In *Proceedings of the 2011 International Conference on Communication, Computing & Security (ICCCS '11)*. ACM, New York, NY, USA, pages 335-338, India, February 2011, DOI=10.1145/1947940.1948010.

Accepted

1. **Sambit Bakshi**, Hunny Mehrotra, and Banshidhar Majhi. Stratified SIFT Matching for Human Iris Recognition. Accepted in *Proceedings of the International Conference on Advances in Computing and Communications (ACC-2011)*. Springer, 2011.

